UNIVERSITY OF HELSINKI REPORT SERIES IN PHYSICS

HU-P-D187

Structure of Relativistic States

Samu Kurki

Division of Elementary Particle Physics
Department of Physics
Faculty of Science
University of Helsinki
Helsinki, Finland

ACADEMIC DISSERTATION

To be presented, with the permission of the Faculty of Science of the University of Helsinki, for public criticism in the auditorium CK112 at Exactum, Gustaf Hällströmin katu 2 B, Helsinki, on November 14th 2011, at 12 o'clock.

Helsinki 2011

ISBN 978-952-10-7068-6 (printed version)
ISSN 0356-0961
ISBN 978-952-10-7069-3 (pdf version)
http://ethesis.helsinki.fi
Helsinki University Print
Helsinki 2011

S. Kurki: Structure of Relativistic States,
University of Helsinki, 2011, 47 pages,
University of Helsinki Report Series in Physics, HU-P-D187
ISSN 0356-0961
ISBN 978-952-10-7068-6 (printed version)
ISBN 978-952-10-7069-3 (pdf version)

Keywords: QCD, factorization, transverse charge densities

Abstract

QCD factorization in the Bjorken limit allows to separate the long-distance physics from the hard subprocess. At leading twist, only one parton in each hadron is coherent with the hard subprocess. Higher twist effects increase as one of the active partons carries most of the longitudinal momentum of the hadron, $x \to 1$. In the Drell-Yan process $\pi N \to \mu^- \mu^+ + X$, the polarization of the virtual photon is observed to change to longitudinal when the photon carries $x_F \gtrsim 0.6$ of the pion. I define and study the "Berger-Brodsky" limit of $Q^2 \to \infty$ with $Q^2(1-x)$ fixed. A new kind of factorization holds in the Drell-Yan process in this limit, in which both pion valence quarks are coherent with the hard subprocess, the virtual photon is longitudinal rather than transverse, and the cross section is proportional to a multiparton distribution.

Generalized parton distributions contain information on the longitudinal momentum and transverse position densities of partons in a hadron. Transverse charge densities are Fourier transforms of the electromagnetic form factors. I discuss the application of these methods to the QED electron, studying the form factors, charge densities and spin distributions of the leading order $|e\gamma\rangle$ Fock state in impact parameter and longitudinal momentum space. I show how the transverse shape of any virtual photon induced process, $\gamma^*(q) + i \to f$, may be measured. Qualitative arguments concerning the size of such transitions have been previously made in the literature, but without a precise analysis. Properly defined, the amplitudes and the cross section in impact parameter space provide information on the transverse shape of the transition process.

Acknowledgements

This thesis is based on research carried out at the Division of Elementary Particle Physics, Department of Physics, University of Helsinki. I gratefully acknowledge the grant from the Jenny and Antti Wihuri Foundation. I also acknowledge the financial support from the Magnus Ehrnrooth Foundation and the Graduate School in Particle and Nuclear Physics (GRASPANP).

First of all, I would like to thank my supervisor Paul Hoyer for his invaluable guidance and advice during my time as a graduate student. He has taught me much about science, and has been an excellent supervisor. I express my gratitude to the pre-examiners of this thesis, Tuomas Lappi and Aleksi Vuorinen, for careful reading of the manuscript and for useful comments. I also thank Matti Järvinen for careful reading of the manuscript and for useful comments, and for fruitful collaboration.

I wish to thank Masud Chaichian and Keijo Kajantie for their advice and encouragement, especially during my earlier years as a graduate student. I am grateful to my colleagues and friends for discussions related to physics and other subjects.

Finally, I would like to thank my parents, brothers, friends, and Jenni, for their constant love and support.

Helsinki, October 2011

Samu Kurki

Contents

List of included papers

The publications included in this thesis are:

I. P. Hoyer, M. Järvinen and S. Kurki
"*Factorization at fixed $Q^2(1-x)$*"
JHEP 10 (2008) 086, arXiv:0808.0626 [hep-ph]

II. P. Hoyer and S. Kurki
"*Transverse shape of the electron*"
Phys. Rev. D 81, 013002 (2010), arXiv:0911.3011 [hep-ph]

III. P. Hoyer and S. Kurki
"*Measuring transverse shape with virtual photons*"
Phys. Rev. D 83, 114012 (2011), arXiv:1101.4810 [hep-ph]

Chapter 1

Introduction

The Standard Model of particle physics accurately describes the strong and electroweak interactions between point-like elementary particles. Elastic $ep \to ep$ scattering experiments performed in the 1950s showed that the proton is not point-like, but has a finite charge radius of $\mathcal{O}(10^{-15}\text{ m})$. In the late 1960s, the observation of Bjorken scaling in inelastic $ep \to eX$ scattering experiments led to the parton model, in which the nucleon is composed of point-like quarks bound together by the strong interaction. Peculiarly, the strength of the strong interaction seemed to diminish in scattering processes involving a large momentum transfer, a property called asymptotic freedom.

Quantum chromodynamics (QCD) emerged as the correct quantum field theory describing the strong interaction, based on the SU(3) color gauge group. The QCD coupling constant decreases logarithmically with the momentum transfer Q^2, allowing the use of perturbation theory in studying processes involving a large momentum transfer. The elementary degrees of freedom in the QCD Lagrangian are quarks and gluons, which are bound together to form color neutral bound states such as the proton and the pion, collectively referred to as hadrons. One of the main challenges of hadron physics is to understand the wealth of phenomena related to hadrons in terms of the quark and gluon degrees of freedom.

The quantum numbers of the hadron, such as its momentum, charge and spin are divided between the constituent partons, and this division is described by certain density distributions. These distributions are measurable in a variety of scattering processes involving hadrons. According to QCD factorization, the inclusive deep inelastic scattering (DIS) $eN \to eX$ cross section is expressed as a product of the hard parton level cross section and the soft parton distribution functions (PDFs) of the hadron. These distributions are universal, in the sense that they do not depend on the scattering process under consideration. QCD factorization is valid in the Bjorken limit of hard processes, in which the hard scale $Q^2 \to \infty$ and the energy transfer ν to the target in its rest frame increases as $\nu \propto Q^2$.

In the leading twist contribution to DIS in the Bjorken limit, only one parton is coherent with the hard virtual photon. Higher twist effects are suppressed by powers of $1/Q^2$, but generally increase as one of the active partons has a longitudinal momentum fraction $x_i \to 1$. In the Drell-Yan (DY) process, $\pi N \to \mu^-\mu^+ + X$, the polarization of the virtual photon producing the muon pair is observed to change to longitudinal when the photon carries a longitudinal momentum fraction $x_F \gtrsim 0.6$ of the pion. In paper I, we defined the "Berger-Brodsky" (BB) limit of $Q^2 \to \infty$ with $Q^2(1-x)$ fixed, and apply it to the DY process. One

of the valence quarks in the pion then has $x_i \to 1$, and the hard photon is coherent with both quarks. We showed that in the DY process a new kind of factorization holds in the BB limit, in which the virtual photon is longitudinal rather than transverse, and the cross section is proportional to a multiparton distribution involving four quark fields, which would be of higher twist in the standard Bjorken limit. The DY amplitude in the BB limit follows simple helicity systematics.

Inclusive DIS provides the most accurate measurement of the longitudinal momentum distributions of partons in the nucleon. Generalized parton distributions (GPDs) contain information on the quark densities in transverse position space through the transverse momentum dependence, but their measurement is more involved than that of the PDFs. Transverse quark densities have been studied using models for the GPDs. The GPDs reduce to the electromagnetic form factors when integrated over the longitudinal momentum fraction x. Thus, the transverse charge density of a nucleon is defined as a two-dimensional Fourier transform of its form factors, a connection that has attracted considerable interest in recent years. The form factors are well defined at all Q^2 and are much easier to measure than the GPDs, which has allowed to plot the nucleon charge densities in transverse position space. Transition (resonance) charge densities have also been considered.

The QED electron has been much studied in the literature, both as a field theory template for QCD hadrons, and for interest in its own right. In paper II, we studied the form factors, transverse densities and spin distributions of the leading order $|e\gamma\rangle$ Fock state of the QED electron in impact parameter space. Only transversally compact Fock states contribute to the leading behavior of the Dirac and Pauli form factors, while distributions weighted by the transverse size of the Fock state have divergences, which could affect the color transparency of hadrons rescattering in a nucleus. There is controversy in the literature on how to split the spin of the nucleon into separate contributions from quark and gluon angular momentum. The helicity of the parent electron is conserved for each $|e\gamma\rangle$ Fock state, while the helicities and orbital angular momentum of the daughter electron and photon depend on their impact parameter and longitudinal momentum fraction. We showed that the sign of the electron anomalous magnetic moment can be understood intuitively from the transverse densities, addressing a challenge by Feynman.

Nucleon transverse charge densities are accessed via form factors measured in $\gamma^*(q)+N \to N$ with the resolution $b \sim 1/Q_{\max}$. The process can be thought of as a relativistic analogue of electron microscopy. In paper III, we considered the transverse shape of any virtual photon induced process, $\gamma^*(q) + i \to f$, where the initial and final states can consist of several hadrons. Qualitative arguments concerning the effective size of the region in transverse space where such transitions take place have been made literature, but without quantitative verification. We showed how a specific Fourier transform of the $\gamma^*(q) + N \to f$ transition amplitude measures the transverse shape of the transition process, and is given by the overlap of the light-front wave functions of the initial and final state. Only Fock states that are common to both the initial and final state contribute to the transition amplitude. The Fourier transformed cross section reflects the difference between the impact parameters of the quark struck in the amplitude and its complex conjugate.

This thesis is organized as follows. In chapter 2, I discuss the properties of QCD and hadron structure. I review factorization in the Bjorken limit, using DIS as an example. I discuss PDFs and GPDs as equal light-front time matrix elements. In chapter 3, I review

the electromagnetic form factors of nucleons. I discuss how transverse densities are obtained from the GPDs, and that the nucleon transverse charge densities are Fourier transforms of the form factors. In chapter 4, I discuss high x processes and the BB limit of $Q^2 \to \infty$ with $Q^2(1-x)$ fixed. I explain how factorization in the DY process $\pi N \to \mu^- \mu^+ + X$ differs from usual QCD factorization in this limit, leading to a longitudinal virtual photon and a multiparton distribution at leading order. In chapter 5, I discuss the form factors, charge densities and spin distributions of the leading order $|e\gamma\rangle$ Fock state of the QED electron. I show how to obtain the form factors from the charge densities, leading to an intuitive argument on the sign of the electron anomalous magnetic moment. In chapter 6, I discuss the possibility of measuring the transverse shape of any virtual photon induced transition process, $\gamma^*(q)+i \to f$. I show how a specific Fourier transform of the *amplitude* measures the transverse shape of the transition, and that the Fourier transformed *cross section* reflects the difference between the impact parameters of quark struck in the amplitude and its complex conjugate. Conclusions and outlook are given in chapter 7.

Chapter 2

QCD and parton distributions

In this chapter I discuss the properties of quantum chromodynamics, and the prospects and challenges related to the study of hadrons. I review factorization and parton distribution functions, using deep inelastic scattering as an example. I discuss transverse momentum distributions and generalized parton distributions. I review the method of light-front quantization, concentrating on the Fock expansion in terms of the light-front wave functions of hadrons.

2.1 QCD and hadron structure

Quantum chromodynamics (QCD) is strongly believed to be the correct quantum field theory describing the strong interaction, one of the four fundamental forces. QCD is a local gauge theory based on the non-abelian SU(3) symmetry group, with the Lagrangian density

$$\mathcal{L}_{\rm QCD}(x) = \sum_{\rm flavors} \bar{q}_A(x)(i\not{D}_{AB} - m\,\delta_{AB})q_B(x) - \frac{1}{4}G^a_{\mu\nu}(x)G^{\mu\nu}_a(x) \tag{2.1}$$

where $q_A(x)$ and $G^a_{\mu\nu}(x)$ are the quark field and gluon field strength operators, respectively. Due to the color confining nature of QCD, the degrees of freedom present in the Lagrangian (2.1), namely, quarks and gluons, are not observed as free particles in nature. Through the strong interaction, quarks and gluons form color neutral bound states known as hadrons, such as the proton and the pion. One of the main challenges in the study of QCD and hadron physics is to understand the wealth of phenomena related to hadrons in terms of the basic quark and gluon degrees of freedom. For example, one may ask, how does the complex spectrum of hadron masses arise from the simple Lagrangian (2.1), a question to which so far only numerical lattice studies of QCD [1, 2] have been able to provide answers. QCD inspired phenomenology such as the nonrelativistic quark model [3, 4] have also been successful.

As mentioned, hadrons are composite particles of quarks and gluons, collectively referred to as partons. The measurable properties of the hadron, such as its momentum, charge, and spin, are divided nontrivially between the constituent partons. This division is described by certain density distributions, which can be measured in a variety of scattering processes involving hadrons. Possibly the best-known examples are the parton distribution functions (PDFs) of the hadron, which describe the distribution of longitudinal momentum between

the partons. The knowledge of the PDFs of the proton is of practical importance in the analysis of hard scattering, for example at the CERN LHC. Much of this chapter is devoted to reviewing the theoretical properties of the PDFs and other related distributions, and their definitions as equal light-front time matrix elements.

2.2 Factorization and DIS

Perturbation theory is one of the key tools in the study of scattering processes. In perturbation theory, one expands the scattering amplitude in powers of the coupling constant of the theory, which is thus assumed to be sufficiently small. Each term in the expansion can be calculated using Feynman rules, which are derived from the Lagrangian of the theory. Perturbation theory works extremely well in the case of quantum electrodynamics (QED). The property of asymptotic freedom allows the application of perturbation theory in QCD if the scattering process has some high momentum scale Q^2. (See [5] for a review on QCD perturbation theory). In chapter 3, I will discuss the transverse charge densities of hadrons, the study of which does not depend on having such a high scale.

In addition to asymptotic freedom, factorization is an integral tool in the study of scattering processes involving hadrons. Factorization describes the incoherence between the long distance, soft dynamics involving momenta $Q \lesssim \Lambda_{\rm QCD} \sim 200\,\text{MeV}$, and the short distance, hard dynamics with $Q \gg \Lambda_{\rm QCD}$. The separation is in practice done at some factorization scale $\Lambda_{\rm QCD} \ll \mu_{\rm F} \ll Q$, the dependence on which vanishes if one takes all orders of perturbation into account. The cross section is then expressed as a product of the hard, parton level cross section, and the soft PDFs and fragmentation functions of the hadrons. The PDFs and fragmentation functions are universal, in the sense that they do not depend on the scattering process under consideration. (See [6] for a review on QCD factorization).

Inclusive deep inelastic scattering (DIS), $e{+}p \to e{+}X$, is a classic example of factorization, and it also provides the most accurate measurement for the PDFs of the proton (see [7] for recent data). In the one-photon approximation, the electron and the proton exchange a virtual photon, and the hard scale is given by the virtuality of the photon, $Q^2 = -q^2$, which thus needs to be large. Factorization is valid in the Bjorken limit of

$$Q^2 \to \infty, \quad x_{\rm Bj} = \frac{Q^2}{2P\cdot q} \text{ fixed} \tag{2.2}$$

where q and P are the four-momenta of the photon and the initial proton, respectively. DIS is conveniently analyzed in the "infinite momentum" or light-front (LF) frame, where the photon momentum is along the negative z-axis. In the Bjorken limit (2.2), the LF energy q^- of the photon is $\mathcal{O}(Q^2)$, while q^+ remains finite ($q^\pm = q^0 \pm q^3$). Due to the phase factor $\exp(i\,q\cdot x)$ of the photon propagator, the photon probes the proton at an instant of LF time $x^+ = t + z \lesssim 1/q^- \to 0$. Using completeness of states at $x^+ \simeq 0$, the DIS cross section is given by the discontinuity of the forward scattering amplitude. The leading twist term for $Q^2 \to \infty$ is given by the "handbag diagram" (see Fig. 2.1), while other higher twist contributions are suppressed by powers of $1/Q^2$. The DIS cross section is then given by the

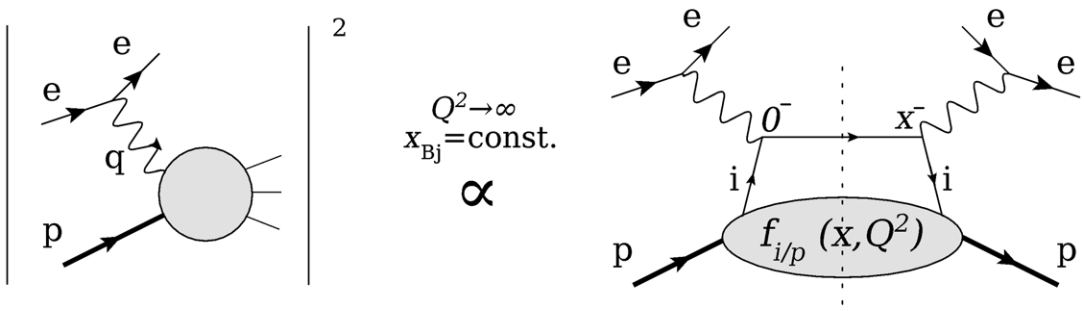

Figure 2.1: The leading term for the DIS cross section in the Bjorken limit (2.2) is given by the handbag diagram, where the photon vertices in the amplitude and its complex conjugate are separated by a lightlike distance $x^+ \simeq 0$.

convolution of the PDF $f_{i/p}(x, Q^2)$ and the hard cross section $\hat{\sigma}$,

$$\sigma_{\rm DIS} = \sum_i \int_0^1 dx\, f_{i/p}(x, Q^2)\, \hat{\sigma}(e + i \to e + i) \tag{2.3}$$

where the struck parton has $p_i^+ = xP^+$, $x \simeq x_{\rm Bj}$ at leading twist, and the PDF is the equal LF time matrix element

$$f_{q/p}(x, Q^2) = \frac{1}{8\pi} \int dx^-\, e^{-ixP^+x^-/2}\, \langle p|\bar{q}(x^-)\gamma^+ W[x^-, 0]q(0)|p\rangle|_{x^+\simeq 0,\, x_\perp \sim 1/Q} \tag{2.4}$$

which indeed only depends on the proton state $|p\rangle$, as required by universality. The transverse resolution $x_\perp \sim 1/Q$ induces a calculable, logarithmic dependence on Q^2. The Wilson line $W[x^-, 0]$ in the PDF (2.4) describes the soft rescattering of the struck quark and the proton within the finite distance $x^- \lesssim 1/(m_q x)$, an effect of which can not be neglected even by choosing the gauge $A^+ = 0$. Thus, the PDFs are not to be strictly interpreted as parton probabilities [8].

2.3 TMDs and GPDs

In addition to the PDF (2.4), other distributions are obtained at leading twist by increasing the number of measured observables. In semi-inclusive DIS, $e + N \to e + j/h(\vec{l}_\perp) + X$, the transverse momentum $\vec{l}_\perp$ of the final state jet or hadron reflects the distribution of transverse momentum $\vec{k}_\perp$ of the struck quark inside the nucleon (see Fig. 2.2). Similarly as the PDF, the transverse momentum distribution (TMD) is defined as the equal LF time matrix element

$$\begin{aligned} f_{q/N}(x, \vec{k}_\perp) &= \frac{1}{8\pi} \int dx^- \frac{d^2\vec{x}_\perp}{(2\pi)^2}\, e^{-ixP^+x^-/2 + i\vec{k}_\perp \cdot \vec{x}_\perp} \\ &\times \langle N|\bar{q}(x^-, \vec{x}_\perp)\gamma^+ W[x^-, \vec{x}_\perp; 0]q(0)|N\rangle|_{x^+\simeq 0} \end{aligned} \tag{2.5}$$

which then measures the longitudinal momentum fraction and the transverse momentum of the struck quark, and reduces to the PDF (2.4) if integrated over $\vec{k}_\perp$. The distribution

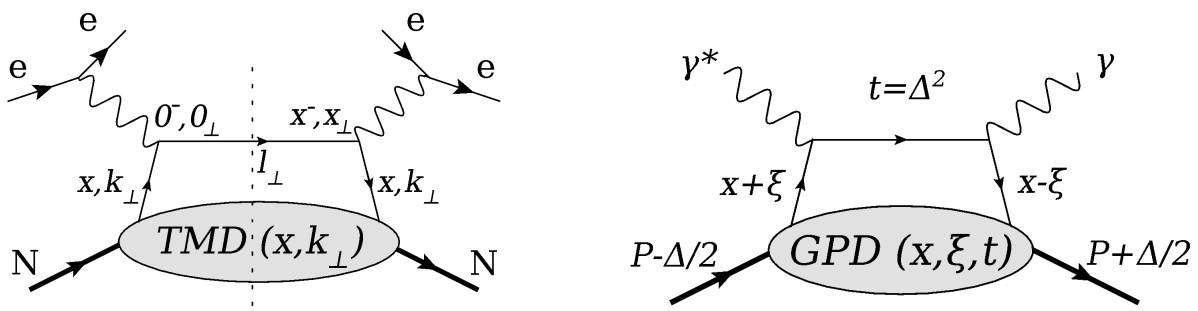

Figure 2.2: Left: The TMD $f_{q/p}(x, \vec{k}_\perp)$ probes the longitudinal momentum fraction x and transverse momentum $\vec{k}_\perp$ of quarks in the nucleon. Right: The GPDs $H(x, \xi, t)$ and $E(x, \xi, t)$ correspond to the lower vertex of the non-forward amplitude shown in the figure.

(2.5) is unpolarized; Assigning definite helicity or transverse spin for the nucleon and/or the struck quark leads to several other TMDs, which reflect correlations between the spin polarization vectors and $\vec{k}_\perp$. (See [9] for a review on TMDs). Factorization for the TMDs is less clear-cut than for the PDF, essentially because the Wilson line $W[x^-, \vec{x}_\perp; 0]$ in (2.5) affects the transverse momentum of the final state jet. This rescattering effect is sensitive to the environment of the scattering process, making the TMDs process dependent, breaking universality [10]. The size of this factorization breaking effect is unclear, however.

Generalized parton distributions (GPDs) are non-forward equal LF time matrix elements of the PDF operator in (2.4), which are functions of the average longitudinal momentum fraction x between the struck parton in the initial and final state, the skewness ξ which measures their difference, and the momentum transfer t between the initial and final state nucleon (see Fig. 2.2). The GPDs $H(x, \xi, t)$ and $E(x, \xi, t)$ are defined through the relation

$$\frac{1}{8\pi}\int dz^- \, e^{imxz^-/2}\langle P + \frac{1}{2}\Delta|\bar{q}(-\frac{z}{2})\gamma^+ W[-\frac{1}{2}z^-, \frac{1}{2}z^-]q(\frac{1}{2}z)|P - \frac{1}{2}\Delta\rangle_{z^+=z_\perp=0}$$
$$= \frac{1}{2P^+}\bar{u}(P + \frac{1}{2}\Delta)\Big[H(x,\xi,t)\gamma^+ + E(x,\xi,t)\, i\sigma^{+\nu}\frac{\Delta_\nu}{2m}\Big]u(P - \frac{1}{2}\Delta) \qquad (2.6)$$

where $\xi = x_{Bj}/(2 - x_{Bj})$ and $t = \Delta^2$. Factorization is valid for $|t| \ll Q^2$, which leads to the handbag diagram shown in Fig. 2.2. The physical content of the GPDs is quite extensive: For $\xi \neq 0$, they measure the coherence between partons of different longitudinal momentum, and hence, longitudinal momentum correlations in the nucleon. (See [11] for a review on GPDs). Through the momentum exchange t, the GPDs contain information on the parton distributions in transverse space, a subject we will return to later in chapter 3. Ji's sum rule [12], essentially the statement that the total spin of a nucleon is the sum of the angular momenta of the quarks and gluons, is expressed using the GPDs $H(x, \xi, t)$ and $E(x, \xi, t)$. As in the case of the TMDs, one may also vary the helicities of the nucleon, producing the helicity flip GPDs $\tilde{H}(x, \xi, t)$ and $\tilde{E}(x, \xi, t)$. The GPDs contain all the information encoded in the PDFs and form factors of the nucleon, as they satisfy

$$\lim_{t\to 0,\, \xi\to 0} H(x, \xi, t) \;\; = \;\; f(x)$$

$$\begin{aligned} \forall\xi: \quad \int_{-1}^{1} dx\, H(x,\xi,t) &= F_1(t) \\ \forall\xi: \quad \int_{-1}^{1} dx\, E(x,\xi,t) &= F_2(t) \end{aligned} \tag{2.7}$$

where $F_1(t)$ and $F_2(t)$ are the Dirac and Pauli form factors of the nucleon, respectively, which we will discuss in detail in chapter 3. Measuring the GPDs is more involved than the PDFs, and while ξ and t are fixed by kinematics, x is integrated over in most observables. The GPDs are accessible at amplitude level in deeply virtual compton scattering, $e + N \to e + \gamma + N$ (see [13] for a review).

2.4 Light-front quantization

The matrix elements appearing in the definitions of the PDFs (2.4), TMDs (2.5) and GPDs (2.6) are matrix elements between nucleon states at the same light-front (LF) time $x^+ \simeq 0$. This leads to the method of LF quantization, in which the nucleon states are also quantized at fixed LF time $x^+ = 0$. (See [14] for a review on LF quantization). The hadron is concisely described in terms of its constituent quarks and gluons using the LF Fock expansion,

$$\begin{aligned} |P^+, \vec{p}_\perp, \lambda\rangle_{x^+=0} &= \sum_{n,\lambda_i} \prod_{i=1}^{n} \Big[\int_0^1 \frac{dx_i}{\sqrt{x_i}} \int \frac{d^2\vec{k}_i}{16\pi^3} \Big] 16\pi^3 \delta(1 - \sum_{i=1}^{n} x_i) \delta^{(2)}(\sum_{i=1}^{n} \vec{k}_i) \\ &\times \psi_n^\lambda(x_i, \vec{k}_i, \lambda_i) |n; x_i P^+, x_i \vec{p}_\perp + \vec{k}_i, \lambda_i\rangle \end{aligned} \tag{2.8}$$

where $\psi_n^\lambda(x_i, \vec{k}_i, \lambda_i)$ are the LF wave functions of the hadron, describing the n-parton Fock state. The partons have longitudinal momentum fractions x_i, transverse momenta $\vec{k}_i$ relative to the hadron, and LF helicities λ_i (see Fig. 2.3). The LF wave functions $\psi_n^\lambda(x_i, \vec{k}_i, \lambda_i)$ are independent of the momentum P^+, $\vec{p}_\perp$ of the hadron, and they are thus able to describe a multitude of different scattering processes involving hadrons, as will become apparent in this thesis. Inserting the expansion (2.8) to the expression for the PDF (2.4), neglecting the

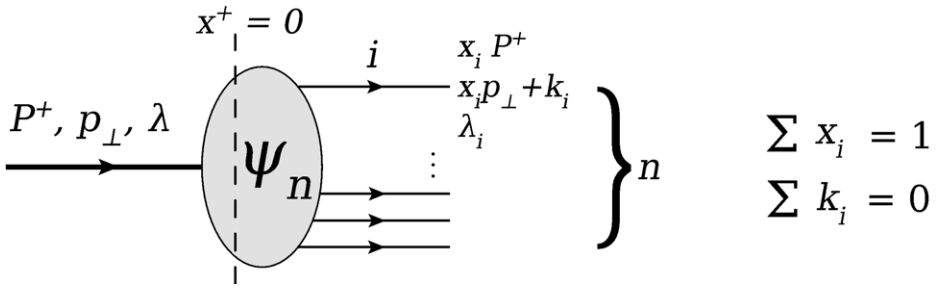

Figure 2.3: The LF Fock expansion describes the hadron at $x^+ = 0$ in terms of its constituent partons.

Wilson line and the logarithmic Q^2 dependence, the PDF is

$$\begin{aligned} f_{q/N}(x) &= \sum_{n,\lambda_i} \prod_{i=1}^{n} \Big[\int_0^1 dx_i \int \frac{d^2\vec{k}_i}{16\pi^3} \Big] 16\pi^3 \delta(1 - \sum_{i=1}^{n} x_i) \delta^{(2)}(\sum_{i=1}^{n} \vec{k}_i) \\ &\times |\psi_n^N(x_i, \vec{k}_i, \lambda_i)|^2 \sum_k \delta(x_k - x) \end{aligned} \tag{2.9}$$

where the Fock state only contributes if it contains a quark with $x_k = x$. The PDF $f_{q/N}(x)$ is process independent by universality, and so are the LF wave functions of the nucleon $\psi_n^N(x_i, \vec{k}_i, \lambda_i)$. The absolute square of the LF wave function in (2.9) allows us to regard the PDF as a probability density of finding quarks with the longitudinal momentum fraction x. The TMD (2.5), again neglecting the rescattering in the target, is similarly

$$\begin{aligned} f_{q/N}(x, \vec{k}_\perp) &= \sum_{n,\lambda_i} \prod_{i=1}^{n} \Big[\int_0^1 dx_i \int \frac{d^2\vec{k}_i}{16\pi^3} \Big] 16\pi^3 \delta(1 - \sum_{i=1}^{n} x_i) \delta^{(2)}(\sum_{i=1}^{n} \vec{k}_i) \\ &\times |\psi_n^N(x_i, \vec{k}_i, \lambda_i)|^2 \sum_k \delta(x_k - x) \delta^{(2)}(\vec{k}_k - \vec{k}_\perp) \end{aligned} \tag{2.10}$$

which can then be interpreted as the probability density of finding quarks with the longitudinal momentum fraction x and transverse momentum $\vec{k}_\perp$ in the nucleon. The GPDs and the form factors of the nucleon can also be expressed in terms of the LF wave functions, allowing their description in terms of the Fock states, which we will return to in the next chapter.

Chapter 3

Form factors and transverse densities

In this chapter I review the properties of the electromagnetic form factors of hadrons, and their measurement in elastic scattering processes. I discuss their interpretation in terms of their parton constituents using the LF Fock expansion. I explain the relation between the GPDs and transverse quark densities. I review the transverse charge densities of hadrons as two-dimensional Fourier transforms of the form factors, also giving a partonic interpretation in terms of the LF Fock states. I show some results that have been obtained for the nucleon using the method of charge densities.

3.1 Elastic processes and form factors

The standard PDFs discussed in chapter 2 are measured in the inclusive process $e+N \to e+X$ assuming that the virtuality of the exchanged photon Q^2 is large enough for factorization to hold. The elastic scattering process $e + N \to e + N$ is also of significant importance to the study of hadrons: For example, the finite size of the proton was inferred from data on elastic electron-proton scattering [15]. In the one-photon approximation, by Lorentz and gauge invariance, the $N + \gamma^* \to N$ scattering amplitude is expressed using the Dirac F_1 and Pauli F_2 form factors (see Fig. 3.1), which depend only on the virtuality of the photon $Q^2 = -q^2$,

$$\begin{aligned} A^{\mu}_{\lambda,\lambda'} &\equiv \langle P + \frac{1}{2}q, \lambda' | \, J^{\mu}(0) \, | P - \frac{1}{2}q, \lambda \rangle \\ &= \bar{u}(P + \frac{1}{2}q, \lambda') \Big[F_1(Q^2)\gamma^{\mu} + F_2(Q^2) \frac{i}{2m} \sigma^{\mu\nu} q_{\nu} \Big] u(P - \frac{1}{2}q, \lambda) \end{aligned} \tag{3.1}$$

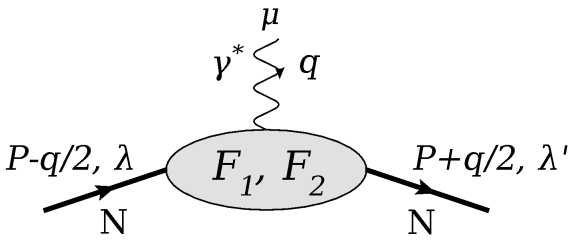

Figure 3.1: The $N + \gamma^* \to N$ scattering amplitude is given by the form factors F_1 and F_2.

where $J^\mu(0) = \sum_q e_q\, \bar{q}(0)\gamma^\mu q(0)$ is the photon electromagnetic current, e_q being the fractional electric charge of the quark. Unlike the PDFs, the form factors are well defined at all values Q^2 of the exchanged momentum, and there is a wealth of data on $F_1(Q^2)$ and $F_2(Q^2)$ of the nucleon, parametrized in various ways (see [16] for recent data). The electron form factors are calculable in QED perturbation theory, $F_1^{(e)}(Q^2)$ being infrared divergent, while $F_2^{(e)}(0)$ is equal to the anomalous magnetic moment of the electron which provides precision tests of QED. In the "LF frame" where $q^+ = 0$, the form factors are

$$\begin{aligned} F_1(Q^2) &= \frac{1}{2P^+}\, A^+_{++} \\ F_2(Q^2) &= \frac{m\, e^{-i\phi_q}}{|\vec{q}_\perp| P^+}\, A^+_{+-} \end{aligned} \tag{3.2}$$

explaining why F_1 and F_2 are called the helicity non-flip and helicity flip form factors, respectively. The form factors in (3.2) are matrix elements of the $J^+(0)$ current, making an interpretation in terms of the Fock states possible: Using the LF Fock expansion (2.8) for the states $|P \pm \frac{1}{2}q\rangle$ at $x^+ = 0$, the form factors are given by

$$\begin{aligned} \frac{1}{2P^+} A^+_{\lambda,\lambda'} &= \sum_{n,\lambda_i} \prod_{i=1}^{n} \Big[\int_0^1 dx_i \int \frac{d^2\vec{k}_i}{16\pi^3} \Big] 16\pi^3 \delta(1 - \sum_{i=1}^{n} x_i)\, \delta^{(2)}(\sum_{i=1}^{n} \vec{k}_i) \\ &\times \sum_k e_k\, [\psi_n^{\lambda'}(x_i, \vec{k}'_i, \lambda_i)]^\dagger \psi_n^{\lambda}(x_i, \vec{k}_i, \lambda_i) \end{aligned} \tag{3.3}$$

where $\vec{k}'_k = \vec{k}_k + (1 - x_k)\vec{q}_\perp$ for the struck quark, $\vec{k}'_i = \vec{k}_i - x_i\vec{q}_\perp$ for the spectators, and e_k is the fractional charge of the struck quark [17]. The expression (3.3) is diagonal in the number of partons in the Fock states, since pair production is absent: a photon with $q^+ = 0$ cannot create two partons with $0 < x_i \leq 1$. Since there is only a single photon interaction vertex, the form factors do not contain a Wilson line, making the expression in terms of the LF wave functions (3.3) exact (up to higher order electromagnetic corrections).

3.2 GPDs and transverse densities

The elastic scattering process $e + N \to e + N$ is analogous to the method of electron microscopy, in which electrons are scattered off a target, and the spatial charge density of the target is given by the $3d$ Fourier transform over the exchanged momentum. It is then reasonable to expect that the form factors $F_1(Q^2)$ and $F_2(Q^2)$ provide information on the quark density of the nucleon at any photon virtuality Q^2. However, unlike in electron microscopy, the partons in the nucleon are not static targets, but highly relativistic, and move as fast as the photon probe. This makes the classical interpretation of the $3d$ Fourier transform of the form factors as the charge density of the nucleon incomplete. It has been shown that due to relativistic effects, the pion form factor has no interpretation in terms of a $3d$ charge density [18]. In a frame where the photon moves rapidly in the $-z$ direction, the photon probes the partons in the nucleon at equal LF time $x^+ = 0$. Thus, the charge densities are more accurately defined as an equal LF time matrix element between nucleon states defined at $x^+ = 0$, also allowing an interpretation in terms of the Fock states.

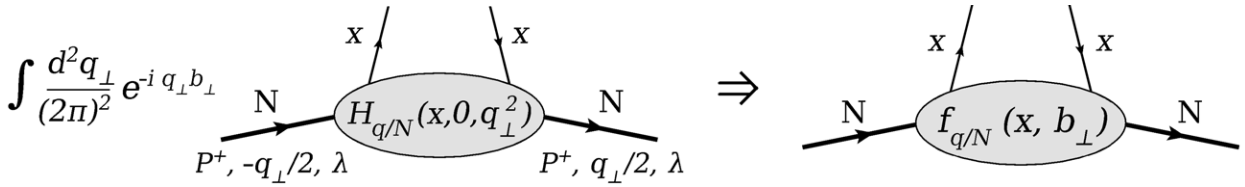

Figure 3.2: The Fourier transform of the GPD gives the distribution of quarks in transverse position space.

The connection between the transverse charge densities and the form factors was first achieved through the GPDs. As mentioned in chapter 2, the GPDs contain information on the spatial quark densities through the dependence on the exchanged momentum $t = \Delta^2$. Choosing the LF frame $q^+ = 0$, ignoring the Wilson line and setting $\xi = 0$, the helicity non-flip GPD is

$$H_{q/N}(x, \vec{q}_\perp^{\,2}) = \frac{1}{8\pi} \int dz^- \, e^{ixP^+z^-/2} \langle P^+, \frac{1}{2}\vec{q}_\perp, \lambda | \bar{q}(-\frac{z}{2})\gamma^+ q(\frac{1}{2}z) | P^+, -\frac{1}{2}\vec{q}_\perp, \lambda \rangle_{z^+=z_\perp=0} \quad (3.4)$$

Fourier transforming over the transverse momentum $\vec{q}_\perp$ leads to the quark density in transverse position space [19] (see Fig. 3.2),

$$f_{q/N}(x, \vec{b}_\perp) = \int \frac{d^2\vec{q}_\perp}{(2\pi)^2} \, e^{-i\vec{q}_\perp \cdot \vec{b}_\perp} \, H_{q/N}(x, \vec{q}_\perp^{\,2}) \quad (3.5)$$

which measures both the longitudinal momentum fraction and the transverse position of the struck quark. As already mentioned, extracting the GPD $H_{q/N}(x, \xi = 0, \vec{q}_\perp^{\,2})$ from scattering data is difficult, and often requires choosing a model for the GPD, leading to model dependence of the quark distribution $f_{q/N}(x, \vec{b}_\perp)$. Such transverse quark densities have been studied in the literature [20, 21].

Using the LF Fock expansion (2.8) for the initial and final nucleon states in the GPD (3.4), one gets

$$\begin{aligned} H_{q/N}(x, \vec{q}_\perp^{\,2}) &= \sum_{n,\lambda_i} \prod_{i=1}^{n} \Big[\int_0^1 dx_i \int \frac{d^2\vec{k}_i}{16\pi^3} \Big] 16\pi^3 \delta(1 - \sum_{i=1}^{n} x_i) \delta^{(2)}(\sum_{i=1}^{n} \vec{k}_i) \\ &\times \sum_k \delta(x - x_k) \, [\psi_n^\lambda(x_i, \vec{k}'_i, \lambda_i)]^\dagger \psi_n^\lambda(x_i, \vec{k}_i, \lambda_i) \end{aligned} \quad (3.6)$$

with $\vec{k}'_k = \vec{k}_k + (1 - x_k)\vec{q}_\perp$ for the struck quark and $\vec{k}_i = \vec{k}_i - x_i\vec{q}_\perp$ for the spectators. To see that the Fourier transformed GPD (3.5) indeed corresponds to a quark density, we write it in terms of the impact parameter LF wave functions of the nucleon, defined as

$$\psi_n^\lambda(x_i, \vec{b}_i, \lambda_i) = \prod_{i=1}^{n} \Big[\int \frac{d^2\vec{k}_i}{16\pi^3} \Big] 16\pi^3 \delta^{(2)}(\sum_{i=1}^{n} \vec{k}_i) \exp\Big(i \sum_{i=1}^{n} \vec{k}_i \cdot \vec{b}_i \Big) \psi_n^\lambda(x_i, \vec{k}_i, \lambda_i) \quad (3.7)$$

which describe a nucleon state with momentum P^+ and transverse "center of momentum" $\vec{b}_N = \sum x_i \vec{b}_i = 0$, whereas the partons in the n-parton Fock state have impact parameters $\vec{b}_i$. The inverse relation of (3.7) is

$$\psi_n^\lambda(x_i,\vec{k}_i,\lambda_i)=\prod_{i=1}^{n}\Big[\int 4\pi\, d^2\vec{b}_i\Big]\frac{1}{4\pi}\delta^{(2)}(\sum_{i=1}^{n}x_i\vec{b}_i)\exp\Big(-i\sum_{i=1}^{n}\vec{k}_i\cdot\vec{b}_i\Big)\psi_n^\lambda(x_i,\vec{b}_i,\lambda_i) \tag{3.8}$$

Inserting this into (3.6) and performing the Fourier transform in (3.5), the quark density in transverse position space becomes

$$\begin{aligned} f_{q/N}(x,\vec{b}_\perp) &= \sum_{n,\lambda_i}\prod_{i=1}^{n}\Big[\int_0^1 dx_i\int 4\pi\, d^2\vec{b}_i\Big]\frac{1}{4\pi}\delta(1-\sum_{i=1}^{n}x_i)\delta^{(2)}(\sum_{i=1}^{n}x_i\vec{b}_i) \\ &\times \sum_k \delta^{(2)}(\vec{b}_\perp-\vec{b}_k)\delta(x-x_k)\,|\psi_n^\lambda(x_i,\vec{b}_i,\lambda_i)|^2 \end{aligned} \tag{3.9}$$

where the Fock state only contributes if it contains a quark with $x_k = x$ and $\vec{b}_k = \vec{b}$, and the absolute square of the wave function enables its interpretation as a probability density.

3.3 Transverse charge densities

As mentioned in chapter 2, the GPDs reduce to the electromagnetic form factors when integrated over the longitudinal momentum fraction, since

$$\int_{-\infty}^{\infty} dx\, \exp(ixP^+z^-/2)=\frac{4\pi}{P^+}\,\delta(z^-) \tag{3.10}$$

The two photon vertices in the GPD essentially coalesce in spacetime (see Fig. 3.3), setting the Wilson line to unity. This motivates to work directly with the form factors: They are much easier to measure than the GPDs, allowing to plot the quark density distributions without model dependence. Unlike the PDFs or the GPDs, the form factors do not depend on having a hard scale $Q^2 \to \infty$; Instead, all values of the photon virtuality contribute to the density distribution, with the expected resolution $b \sim 1/Q_{\max}$. Thus, the transverse charge density of a nucleon with LF helicity $\lambda = \pm\frac{1}{2}$ is defined as the Fourier transform of the form factor [22, 23],

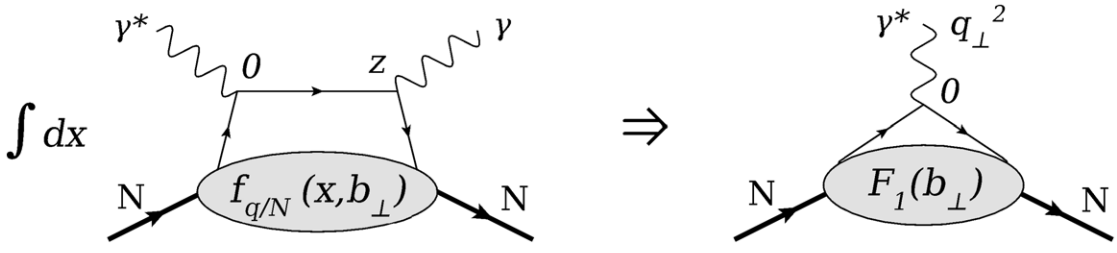

Figure 3.3: The Dirac and Pauli form factors are obtained from the GPDs, here shown for F_1.

$$\begin{aligned}\rho_0(\vec{b}) &\equiv \int \frac{d^2\vec{q}}{(2\pi)^2}\, e^{-i\vec{q}\cdot\vec{b}}\, \frac{1}{2P^+}\langle P^+, \frac{1}{2}\vec{q}, \lambda | J^+(0) | P^+, -\frac{1}{2}\vec{q}, \lambda\rangle \\ &= \int_0^\infty \frac{dQ}{2\pi}\, Q J_0(bQ)\, F_1(Q^2) \end{aligned} \tag{3.11}$$

where the momentum of the virtual photon is $q = (0^+, 0^-, \vec{q})$, J_0 is a Bessel function and $Q^2 = \vec{q}^2$. In terms of the impact parameter LF wave functions (3.7),

$$\begin{aligned}\rho_0(\vec{b}) &= \sum_{n,\lambda_i,k} e_k \prod_{i=1}^n \Big[\int_0^1 dx_i \int 4\pi\, d^2\vec{b}_i\Big] \frac{1}{4\pi}\delta(1 - \sum_{i=1}^n x_i)\delta^{(2)}(\sum_{i=1}^n x_i \vec{b}_i) \\ &\times \delta^{(2)}(\vec{b} - \vec{b}_k)\, |\psi_n^\lambda(x_i, \vec{b}_i, \lambda_i)|^2 \end{aligned} \tag{3.12}$$

By rotational symmetry, the transverse density $\rho_0(\vec{b})$ depends only on $|\vec{b}|$. For a transversely polarized nucleon with spin in the x-direction, one similarly defines

$$\begin{aligned}\rho_x(\vec{b}) &\equiv \int \frac{d^2\vec{q}}{(2\pi)^2}\, e^{-i\vec{q}\cdot\vec{b}}\, \frac{1}{2P^+}\langle P^+, \frac{1}{2}\vec{q}, S_x = +\frac{1}{2} |\, J^+(0)\, | P^+, -\frac{1}{2}\vec{q}, S_x = +\frac{1}{2}\rangle \\ &= \rho_0(\vec{b}) + \sin(\phi_b) \int_0^\infty \frac{dQ}{2\pi}\, \frac{Q^2}{2m}\, J_1(bQ)\, F_2(Q^2) \end{aligned} \tag{3.13}$$

where we used $|S_x = +\frac{1}{2}\rangle = \Big[|\lambda = +\frac{1}{2}\rangle + |\lambda = -\frac{1}{2}\rangle\Big]/\sqrt{2}$, and thus the helicity flip form factor $F_2(Q^2)$ also contributes. The density $\rho_x(\vec{b})$ may also be written in terms of the absolute squares of the wave functions as in (3.12) by replacing $\psi_n^\lambda \to (\psi_n^{\lambda=+1/2} + \psi_n^{\lambda=-1/2})/\sqrt{2}$. The transverse charge densities $\rho_0(\vec{b})$ and $\rho_x(\vec{b})$ of the proton and the neutron are shown in Fig. 3.4, where the authors used parametrized data [24, 25] for the nucleon form factors. The neutron transverse charge density is negative at the origin, whereas in the classical definition of the charge densities as $3d$ Fourier transforms, the neutron charge density is positive [26], a qualitative difference between the two methods. Transition charge densities have also been considered, where the LF matrix element in (3.11) is a transition form factor describing $N + \gamma^* \to N^*$. The transition charge densities have been plotted for $p \to \Delta^+(1232)$ [27] and $p \to N^*(1440)$ [28], both in the unpolarized and polarized cases. In chapter 6, we will consider generalized transverse charge densities describing $i + \gamma^* \to f$, where the initial and final states can consist of several particles.

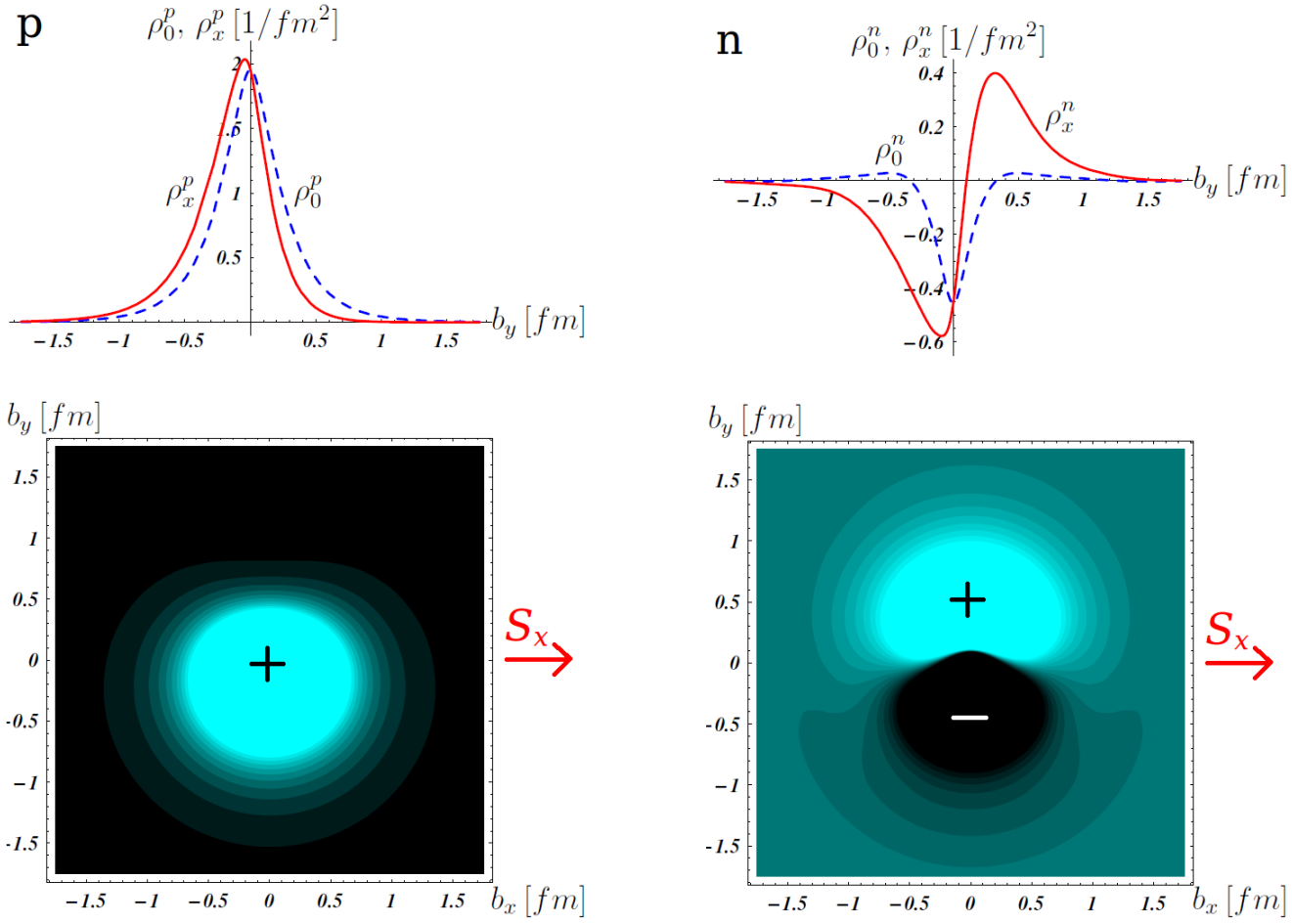

Figure 3.4: Upper row: The transverse charge densities ρ_0 and ρ_x of the proton and the neutron along the b_y axis. The dashed lines correspond to the unpolarized densities (3.11), while the solid lines are for the densities with the nucleon polarized in the x-direction as in (3.13). Lower row: The transverse charge densities for the proton and the neutron polarized in the x-direction. Figures from [27].

Chapter 4

Factorization at fixed $Q^2(1-x)$

Scattering processes have succesfully been analyzed using factorization in the Bjorken limit of $Q^2 \to \infty$, as discussed in chapter 2. At leading twist, only one active parton in each nucleon takes part in the hard subprocess. Qualitatively new features are observed in situations, where one of the active partons in the hadron carries most of its longitudinal momentum, so that the longitudinal momentum fraction $x \to 1$. In the Drell-Yan (DY) process, $\pi N \to \mu^- \mu^+ + X$, the polarization of the virtual photon producing the muon pair is measured to change to longitudinal when the photon carries a longitudinal momentum fraction $x_F \gtrsim 0.6$ of the pion. In paper I, we defined the "Berger-Brodsky" (BB) limit, where the hard scale $Q^2 \to \infty$, while $Q^2(1-x)$ is fixed, and apply it to the DY process. In this limit, one of the valence quarks in the pion has $x \to 1$, and the hard photon is coherent with both quarks. We showed that in the DY process a new kind of factorization holds in the BB limit, in which the virtual photon is longitudinal rather than transverse, and the cross section is proportional to a multiparton distribution involving four quark fields, which would be of higher twist in the Bjorken limit. The DY amplitude in the BB limit follows simple helicity systematics.

4.1 The Berger-Brodsky (BB) limit

The standard factorization between hard and soft subprocesses in scattering reactions is achieved in the Bjorken limit, where a hard scale $Q^2 \to \infty$, while the longitudinal momentum fractions x_i of the active partons are held fixed. The cross section then factorizes into a product of the soft PDF and the hard, parton level cross section. At leading twist, only one parton in each nucleon takes part in the hard subprocess. Higher twist effects are suppressed by powers of $1/Q^2$, but generally increase [29] as $x_i \to 1$ (see Fig. 4.1), implying an increase in the coherence between the active and spectator partons. In the Drell-Yan (DY) process $\pi N \to \mu^+ \mu^- + X$, the polarization of the virtual photon producing the muon pair changes from transverse to longitudinal, when the photon carries a longitudinal momentum fraction $x_F \gtrsim 0.6$ of the pion [30, 31] (see Fig. 4.2). One of the valence quarks in the pion then carries most of the longitudinal momentum of the pion, and the hard photon is coherent with both quarks [32]. A similar change in polarization was observed at high x_F in $\pi N \to J/\psi + X$ [33]. The transverse single-spin asymmetry (SSA) in $pp^\uparrow \to \pi(x_F, k_\perp) + X$, measured by $A_N = (\sigma^\uparrow - \sigma^\downarrow)/(\sigma^\uparrow + \sigma^\downarrow)$, where the $\updownarrow$ arrows indicate the transverse polarization of the

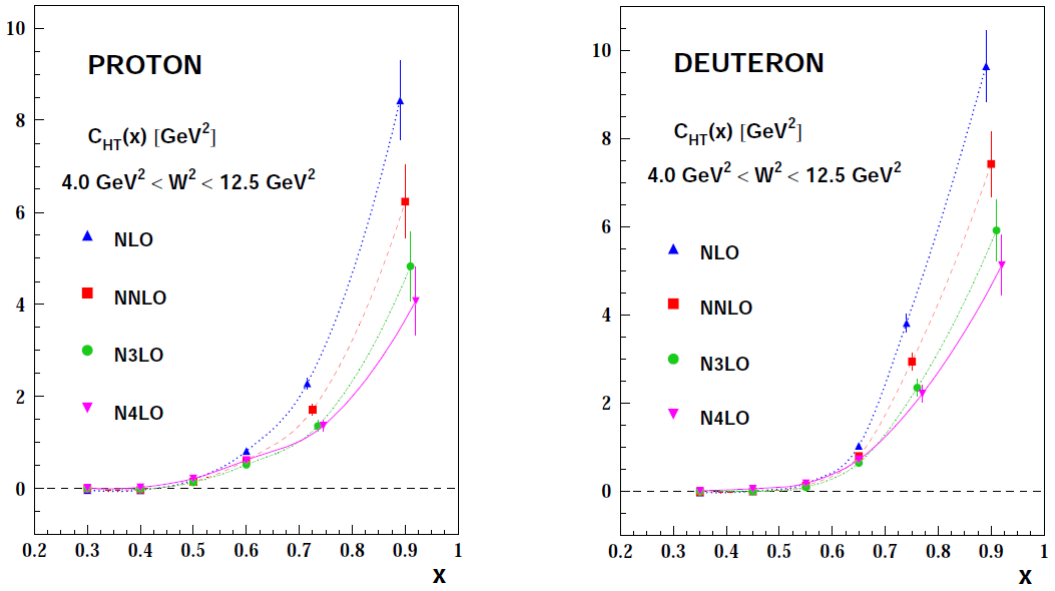

Figure 4.1: The effective higher twist distribution functions $C_{HT}(x)$ of the proton and the deuteron, which represent the higher twist contributions to the proton and deuteron structure functions. The data has been extrapolated from the large W^2 region to the region $4.0\,\mathrm{GeV}^2 \leq W^2 \leq 12.5\,\mathrm{GeV}^2$ using N^nLO analyses. Figures from [29].

proton, was found to increase as a function of x_F [34, 35] (see Fig. 4.2). The SSA also does not decrease as a function of $k_\perp$, whereas the leading twist prediction is $A_N \propto \Lambda_{\rm QCD}/k_\perp$. Generating the SSA requires a helicity flip and a dynamical phase in a subprocess, which is coherent with the high $k_\perp$ parton [36].

To qualitatively understand the onset of coherence between the spectators and the hard subprocess for the Fock state containing the active parton with $x \to 1$, we consider the life-time of such a Fock state, which is inversely proportional to the energy difference between the hadron and the Fock state,

$$2p\Delta E \simeq m_h^2 - \sum_i \frac{p_{i\perp}^2 + m_i^2}{x_i} \tag{4.1}$$

at high momentum p of the hadron. The life-time is determined by the spectators with $x_i \propto 1-x$. If $1-x \simeq \Lambda_{\rm QCD}^2/Q^2$, $2p\Delta E \simeq Q^2$ and the life-time of the Fock state is short, comparable to the duration of the hard subprocess. Hence, the BB limit is defined as

$$Q^2 \to \infty, \qquad Q^2(1-x) = \text{fixed} \tag{4.2}$$

which was initially used to predict the change of polarization in the DY process at high x_F [32]. Later it was shown that in $pp^\uparrow \to \pi(x_F, k_\perp) + X$ a large SSA A_N of $\mathcal{O}(1)$ can arise in the BB limit using a perturbative example calculation [36]. In DIS, $\gamma^* N \to X$, the BB limit of fixed $Q^2(1-x_{\rm Bj})$ corresponds to a fixed hadronic (resonance) mass M_X. The Bloom-Gilman duality is a remarkable equality between the inclusive DIS data with $Q^2 \to \infty$ at fixed $x_{\rm Bj}$, and the exclusive resonance contributions measured at lower Q^2 with fixed M_X (see [37] for a review). The duality suggests that the photon scatters off the same Fock states with the same

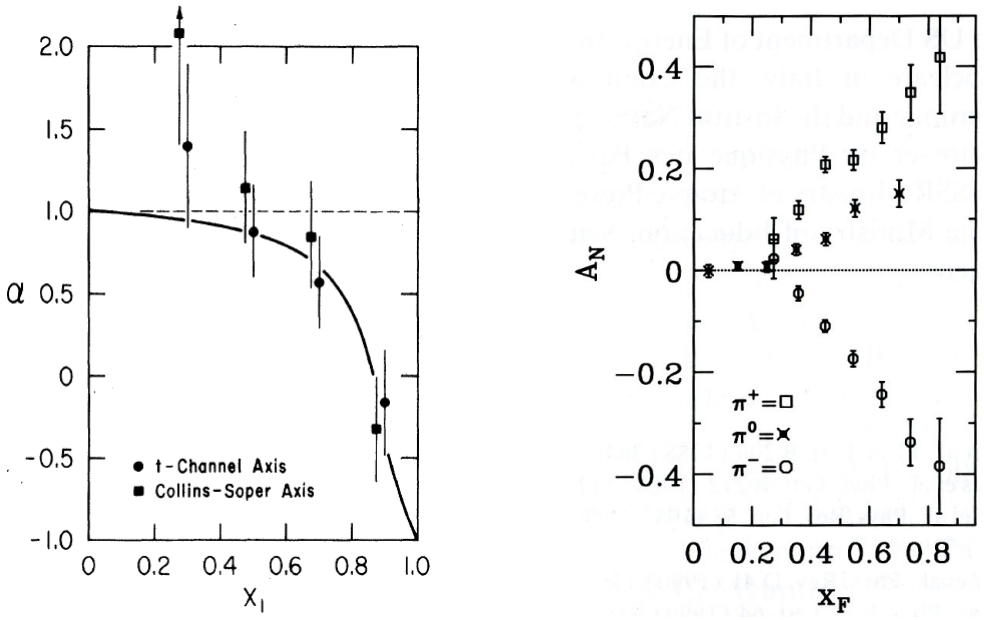

Figure 4.2: Left: Fermilab E615 data for the cross section $\frac{d\sigma}{d\cos\theta} \propto 1 + \alpha\cos^2\theta$ in $\pi^- N \to \mu^+\mu^- + X$, where $Q > 4\,\text{GeV}$ and $p_{\text{lab}} = 263\,\text{GeV/c}$. Figure from [30]. Right: Fermilab E704 data for $A_N(x_F)$ in $pp^\uparrow \to \pi + X$, where $k_\perp$ was integrated from 0.5 GeV to 2.0 GeV for π^0 data and from 0.7 GeV to 2.0 GeV for $\pi^\pm$ data, and $p_{\text{lab}} = 200\,\text{GeV/c}$. Figure from [34].

hard subprocess cross section in $eN \to eX$ and $eN \to eN^*$. The exclusive transition process is coherent over the whole wave function of the nucleon, implying coherence in inclusive processes in the BB limit.

4.2 The Drell-Yan (DY) process in the BB limit

For the DY process $\pi N \to \mu^+\mu^- + X$, according to factorization in the Bjorken limit of $Q^2 = x_1 x_2 s \to \infty$ with x_1, x_2 fixed, the leading twist cross section has the valence contribution

$$\sigma_{\text{DY}} = f_{\bar{q}/\pi}(x_1)\, f_{q/N}(x_2)\, \hat{\sigma}(\bar{q}q \to \gamma^* \to \mu^+\mu^-) \tag{4.3}$$

Only one active parton in the pion and the nucleon takes part in the hard subprocess, which is incoherent with the spectators. The virtual photon producing the muon pair is transverse, since the annihilating quarks are nearly on-shell (see Fig. 4.3). As mentioned, the photon is longitudinally polarized for high x_F, implying that the active parton in the pion has $x \to 1$. In the BB limit of $Q^2 \to \infty$ with $Q^2(1-x_F)$ fixed, the quark in the pion transfers nearly all of its momentum to the antiquark through the exchange of a gluon with virtuality $q_1 = \mathcal{O}(Q^2)$. The antiquark also has virtuality $q_2 = \mathcal{O}(Q^2)$, and the virtual photon is longitudinal. The stopped quark is then coherent with the virtual photon (see Fig. 4.3) [32].

The factorized form of the DY cross section in the BB limit differs from (4.3), as we next discuss. The kinematics are shown in Fig. 4.3. In the nucleon rest frame,

$$k \;=\; (0^+, k^-, \vec{0}_\perp)$$

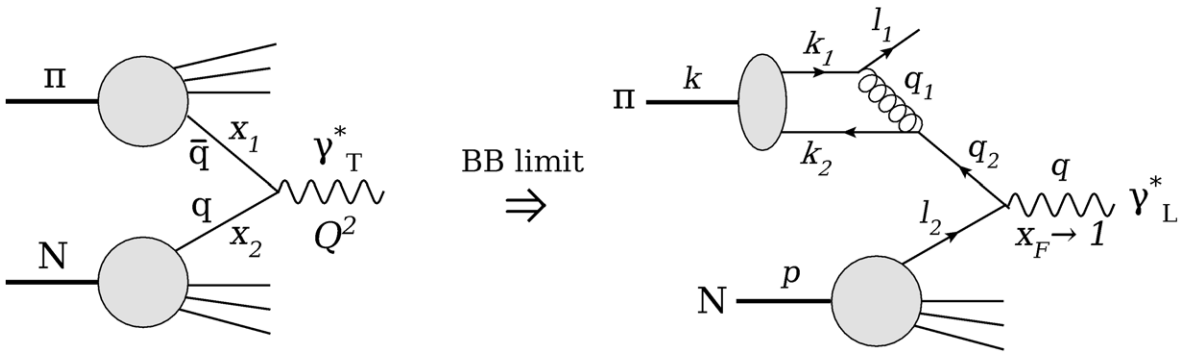

Figure 4.3: The polarization of the virtual photon in DY scattering changes to longitudinal in the BB limit, and the stopped quark is coherent with the hard process.

$$\begin{aligned} p &= (m_N, m_N, \vec{0}_\perp) \\ q &= (Q^2/q^-, q^-, \vec{q}_\perp) \end{aligned} \tag{4.4}$$

where we take $k^- \to \infty$ neglecting the pion mass, and thus $s \simeq m_N k^- \to \infty$. In the BB limit, $x_F \equiv q^-/k^- \to 1$ at fixed $\vec{q}_\perp$, keeping also $x_B \equiv q^+/p^+ = Q^2/s$ and $x_M \equiv Q^2(1-x_F)/(q^+p^-)$ fixed. The hadronic mass is

$$M_X^2 = (k+p-q)^2 \simeq (1-x_B)[s(1-x_F) + m_N^2] - \vec{q}_\perp^{\,2} \tag{4.5}$$

which is thus fixed, and may be small or large depending on $s(1-x_F)$. The momenta of the valence quarks of the pion are

$$\begin{aligned} k_1 &= (0^+, zk^-, \vec{k}_\perp) \\ k_2 &= (0^+, (1-z)k^-, -\vec{k}_\perp) \end{aligned} \tag{4.6}$$

where the transverse momenta $k_\perp^2 \ll Q^2$ are neglected in the hard subprocess. The stopped quark has finite momentum l_1 in the nucleon rest frame, and is connected to the soft matrix element of the nucleon. This is analogous to the analysis of DIS in the target rest frame, where the scattering may be viewed as the splitting of the virtual photon, $\gamma^*(Q^2) \to q\bar{q}$, where the fast quark has momentum fraction $x_q \simeq 1$, and the scattering of the antiquark with finite momentum and $x_{\bar{q}} \sim \Lambda_{\rm QCD}^2/Q^2$ in the target determines the DIS cross section [38, 39]. The quark and gluon virtualities are $q_1^2 \simeq -zk^-l_1^+$ and $q_2^2 \simeq -k^-l_1^+$, which are $\mathcal{O}(Q^2)$. The momenta q_1^-, q_2^- are also $\mathcal{O}(Q^2)$, implying that the hard subprocess occurs in an instant of LF time $|y_1^+ - y_3^+| = \mathcal{O}(1/Q^2) \to 0$, $|\vec{y}_{1\perp} - \vec{y}_{3\perp}| = \mathcal{O}(1/Q) \to 0$. In the hard subprocess, it suffices to take

$$\begin{aligned} l_1 &= (xp^+, 0^-, \vec{0}_\perp) \\ l_2 &= ((x+x_B)p^+, 0^-, \vec{0}_\perp) \end{aligned} \tag{4.7}$$

Thus both valence quarks in the pion effectively reverse their direction along the z-axis, allowing the helicity analysis of section 4.3.

Using perturbative propagators for the gluon q_1 and the quark q_2, and connecting the quarks l_1 and l_2 to the soft matrix element, the scattering amplitudes are given by the

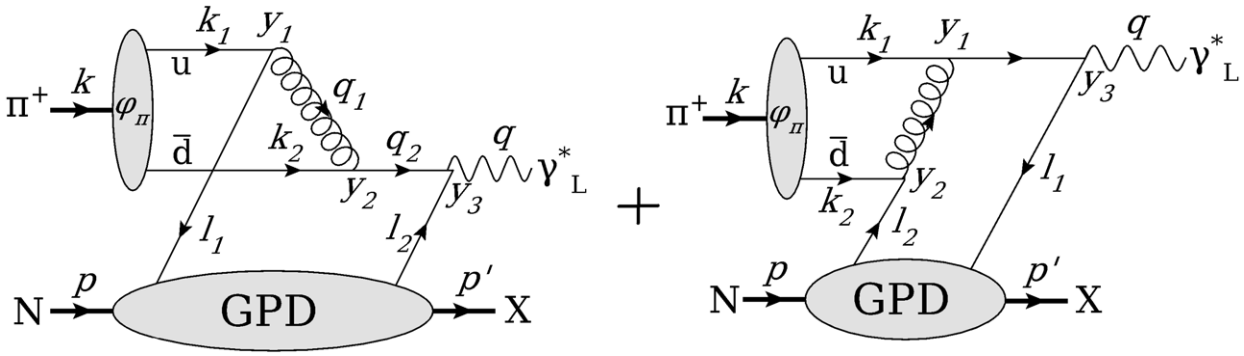

Figure 4.4: The Feynman diagrams contributing to $\pi^+ N \to \gamma^* X$ in the BB limit. The arrows indicate directions of momenta, and the y_i are positions of the interaction vertices.

Feynman diagrams depicted in Fig. 4.4. The pion contributes via its distribution amplitude $\phi_\pi(z)$, and for each final state X, the target matrix element is a transition GPD with skewness $(l_2^+ - l_1^+)/p^+ = x_B$. For $X = N$, the amplitudes correspond to the exclusive DY process $\pi N \to \gamma^* N$ [40], as well as the time-reversed version of deeply exclusive meson production $\gamma^* N \to \pi N$. The factorization discussed in chapter 2 is equally valid for the transition GPDs when $X \neq N$ [41], since $M_X \ll Q$. The scattering amplitude is calculated as

$$\begin{aligned} T(\pi^+ N \to \gamma_L^* X) &= \frac{-ieg^2 C_F}{2\pi Q\sqrt{2N_c}} \int dx\, C(x_B, x) \\ &\times \int dy_1^-\, e^{-iy_1^- xp^+/2} \langle X(p')|\bar{\psi}_u(y_1)\gamma^+\gamma_5\psi_d(0)|N(p)\rangle_{y_1^+ = y_{1\perp} = 0} \end{aligned} \tag{4.8}$$

where

$$C(x_B, x) = \int_0^1 dz\, \phi_\pi(z) \Big[\frac{e_d}{z} \frac{1}{x - i\epsilon} + \frac{e_u}{1-z} \frac{1}{x_B + x + i\epsilon} \Big] \tag{4.9}$$

The amplitude for the production of a transverse photon is suppressed by a factor of $1/Q$, for which we give an intuitive explanation in section 4.3. The inclusive cross section is

$$\sigma(\pi^+ N \to \gamma_L^* X) = \frac{1}{2s} \sum_X \int \frac{dq^- d\vec{q}_\perp^{\,2}}{(2\pi)^3 2q^-} |T(\pi^+ N \to \gamma_L^* X)|^2 (2\pi)^4 \delta^{(4)}(k + p - q - p') \tag{4.10}$$

The completeness sum $\sum_X$ includes summing over p', which is restricted by the delta function. Integrating over $\vec{q}_\perp = -\vec{p}'_\perp$ eliminates the transverse momentum constraint, and the longitudinal delta functions can be incorporated into the soft matrix element as position integrals. The inclusive cross section (4.10) is then given given by a forward multiparton distribution (see Fig. 4.5) depending on the fractional "+" momenta

$$x_B = q^+/p^+, \quad x = l_1^+/p^+, \quad x' = l_1'^+/p^+ \tag{4.11}$$

and the fractional "−" momentum transferred to the inclusive system,

$$x_M = k^-(1 - x_F)/p^-, \qquad \frac{x_B + \vec{q}_\perp^{\,2}/m_N^2}{1 - x_B} \leq x_M < \infty \tag{4.12}$$

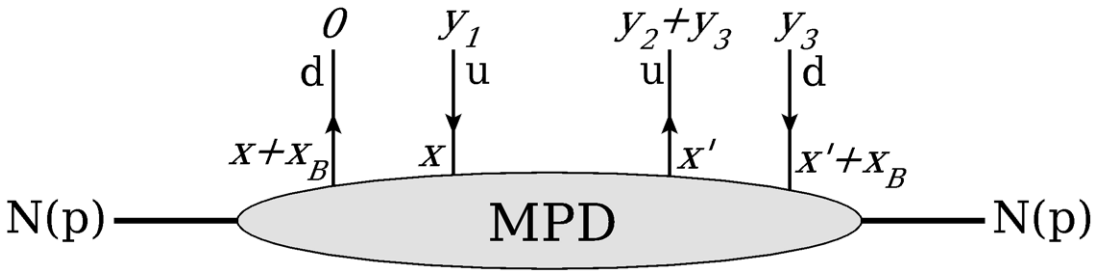

Figure 4.5: The multiparton distribution $f_{d\bar{u}/p}(x_B, x_M, x, x')$ in the inclusive cross section (4.14) involving four quark fields.

The forward multiparton distribution is

$$f_{d\bar{u}/p}(x_B, x_M, x, x') \tag{4.13}$$
$$= \tfrac{1}{4(4\pi)^3} \int dy_1^- dy_2^- dy_3^- dy_3^+ \exp\Big(\tfrac{1}{2} i[-y_1^- l_1^+ + y_2^- l_1'^+ - y_3^- q^+ + y_3^+ x_M p^-]\Big)$$
$$\times \langle N(p)|\bar{\psi}_d(y_3)\gamma^+\gamma_5\psi_u(y_2+y_3)\bar{\psi}_u(y_1)\gamma^+\gamma_5\psi_d(0)|N(p)\rangle_{y_{i\perp}=0,\, y_1^+=y_2^+=0}$$

and the inclusive cross section is

$$\frac{d\sigma(\pi^+ N \to \gamma_L^* X)}{dM_X^2} = \frac{2(eg^2 C_F)^2}{Q^2 s^2 (1-x_B) N_c} \int dx dx'\, C(x_B, x) C^*(x_B, x') f_{d\bar{u}/p}(x_B, x_M, x, x') \tag{4.14}$$

The dependence on x_M separates $f_{d\bar{u}/p}(x_B, x_M, x, x')$ from usual higher twist multiparton distributions [42]. In the Bjorken limit at fixed x_F, we would have $x_M \to \infty$ and thus $y_3^+ = 0$. The u-quark in the pion then has $l_1^- = k^-(1-x_F) \to \infty$ and forms a jet in the final system X. The GPD in the scattering amplitude (4.8) then reduces to the standard d-quark PDF, as expected.

4.3 DY helicity systematics

In the BB limit of $\pi^+ N \to \gamma^* X$, the photon carries the helicity of the pion $\lambda = 0$, which intuitively follows from the fact that the virtual photon is coherent with the whole Fock state of the pion. This argument does not work for the proton induced DY process $pN \to \gamma^* X$, since $|\Delta\lambda| \geq 1/2$ for a transverse or longitudinal photon. The DY scattering amplitude in the BB limit follows simple helicity systematics, since:

1. All transverse momenta are restricted, $k_\perp$, $q_\perp$, $l_\perp \sim \Lambda_{\rm QCD}$.
2. Angular momentum $J_z = S_z + L_z$ is conserved in each vertex.
3. The helicities of the quark lines are conserved up to terms m_q/Q.

The helicities of the virtual quark and the gluon are followed by expressing their propagators as sums over helicities using the Dirac u and v spinors, as well as the polarization vectors ϵ_λ^μ

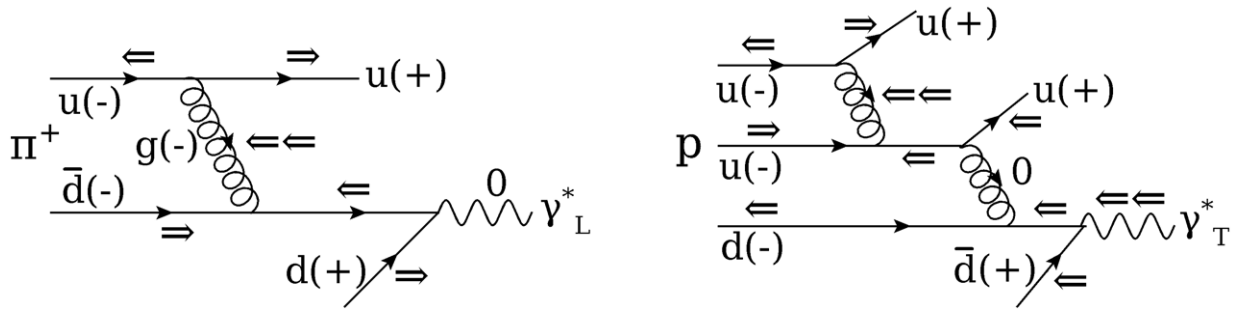

Figure 4.6: Left: Helicity analysis for $\pi^+ N \to \gamma^* X$, where the particles have momenta in the $\pm z$ direction as shown in the parentheses. The double arrows indicate the S_z of the particles in units of $\frac{1}{2}\hbar$. Right: Helicity analysis for $pN \to \gamma^* X$ in the same notation.

of the gluon,

$$\begin{aligned} \frac{\not{p}+m}{p^2+m^2-i\epsilon} &= \sum_{s=\pm\frac{1}{2}} \frac{1}{2E_p}\Big[\frac{u(\vec{p},s)\bar{u}(\vec{p},s)}{p^0-E_p+i\epsilon}+\frac{v(-\vec{p},s)\bar{v}(-\vec{p},s)}{p^0+E_p-i\epsilon}\Big] \\ -g^{\mu\nu}+\frac{k^\mu k^\nu}{k^2} &= \sum_{\lambda=\pm1,0} \epsilon^\mu_\lambda(k)\epsilon^\nu_\lambda(k)^* \end{aligned} \tag{4.15}$$

In the leading contribution to the scattering amplitude, the helicities are then obtained by simple addition. The analysis for one of the Feyman graphs of the pion induced DY process is shown in Fig. 4.6, where the photon is longitudinal. Using a three-quark Fock state for the proton, the analysis predicts that the photon is transverse in $pN \to \gamma^* X$. The analysis for one of the eight Feynman graphs is shown in Fig. 4.6. In a similar case of the exclusive $\bar{p}N \to \gamma^*\pi$ process, the photon was also found to be transversely polarized [43].

Chapter 5

Transverse shape of the electron

Transverse charge densities given by elastic nucleon and $N \to N^*$ transition form factors have been studied using GPD models, as discussed in chapter 3. In paper II, we applied these methods to the QED electron, which serves as a field theory model for QCD hadrons, and is of interest in its own right. We studied the form factors, transverse densities and spin distributions of the leading order $|e\gamma\rangle$ Fock state of the QED electron in impact parameter space. The LF wave functions of the $|e\gamma\rangle$ state are calculated in impact parameter space, which allows closed form expressions for the electron distributions. The Dirac and Pauli form factors are expressed in terms of the charge densities, which allowed us to study the transverse size of the Fock states contributing to the electron form factors at any Q^2. Only transversally compact Fock states contribute to the leading behavior of the Dirac and Pauli form factors, while distributions weighted by the transverse size of the Fock state have divergences, which could affect the color transparency of hadrons rescattering in a nucleus. The helicity of the parent electron is conserved for each $|e\gamma\rangle$ Fock state, while the helicities and orbital angular momentum of the daughter electron and photon depend on their impact parameter and longitudinal momentum fraction. We showed that the sign of the electron anomalous magnetic moment can be understood intuitively from the transverse densities, addressing a challenge by Feynman.

5.1 Electron distributions in impact parameter space

As discussed in chapter 3, GPDs correspond to parton densities in longitudinal momentum fraction x and impact parameter $\vec{b}$ when Fourier transformed over the transverse momentum. The transverse charge densities are x-integrated GPDs, and are obtained from the Fourier transformed electromagnetic form factors. The nucleon and transition charge densities have been studied using form factor data. In this chapter, I apply these methods to the QED electron. The leading order $|e\gamma\rangle$ Fock state of the electron has been used as a field theory model for QCD hadrons in several studies [44, 45, 46, 47, 48]. The GPDs were expressed in terms of the LF wave functions in impact parameter space, which are calculable for the electron in QED perturbation theory. The LF wave functions of the $|e\gamma\rangle$ Fock state in momentum space in the $A^+ = 0$ gauge are given in [49]. For an electron localized at $\vec{b} = 0$, we define $x_e \equiv x = 1 - x_\gamma$, $\vec{b}_e \equiv \vec{b} = -(1-x)\vec{b}_\gamma/x$ and denote $m_e \equiv m$ (see Fig. 5.1).

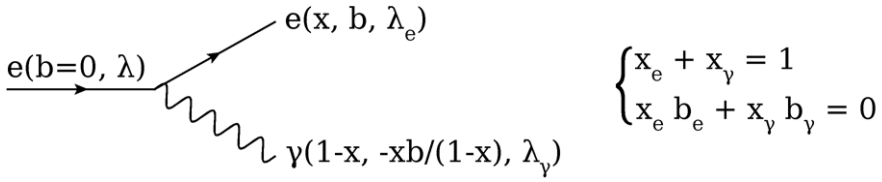

Figure 5.1: The first order $|e\gamma\rangle$ Fock state of the electron localized at $\vec{b} = 0$.

The impact parameter wave functions of the $|e\gamma\rangle$ Fock state are expressed in terms of the momentum space ones as in (3.7),

$$\psi^{\lambda}_{\lambda_e,\lambda_\gamma}(x,\vec{b}) = \int \frac{d^2\vec{k}}{16\pi^3} \exp\Big[i\frac{\vec{b}\cdot\vec{k}}{1-x}\Big]\psi^{\lambda}_{\lambda_e,\lambda_\gamma}(x,\vec{k}) \tag{5.1}$$

Using the identities

$$\int_0^{2\pi} d\phi\, e^{iz\cos\phi}e^{in\phi} = 2\pi i^n J_n(z), \quad \int_0^\infty dt\, \frac{t^{\nu+1}J_\nu(at)}{(t^2+z^2)^{\mu+1}} = \frac{a^\mu z^{\nu-\mu}}{2^\mu\Gamma(\mu+1)}K_{\nu-\mu}(az) \tag{5.2}$$

we have, denoting $\vec{b} = b(\cos\phi_b,\, \sin\phi_b)$ and $\lambda = \pm\frac{1}{2} \equiv \pm$,

$$\begin{aligned}
\psi^+_{+1/2,+1}(x,\vec{b}) &= [\psi^-_{-1/2,-1}(x,\vec{b})]^\dagger = -i\frac{em\sqrt{1-x}}{4\sqrt{2}\pi^2}e^{-i\phi_b}K_1(mb) \\
\psi^+_{+1/2,-1}(x,\vec{b}) &= [\psi^-_{-1/2,+1}(x,\vec{b})]^\dagger = i\frac{em\sqrt{1-x}}{4\sqrt{2}\pi^2}x\, e^{+i\phi_b}K_1(mb) \\
\psi^+_{-1/2,+1}(x,\vec{b}) &= [\psi^-_{+1/2,-1}(x,\vec{b})]^\dagger = -\frac{em\sqrt{(1-x)}}{4\sqrt{2}\pi^2}(1-x)K_0(mb) \\
\psi^+_{-1/2,-1}(x,\vec{b}) &= [\psi^-_{+1/2,+1}(x,\vec{b})]^\dagger = 0
\end{aligned} \tag{5.3}$$

There is no explicit factor of m associated with the wave functions in which the electron helicity flips; The dependence on m appears through the index n of the modified Bessel function $K_n(mb)$. Using (3.9), the wave functions (5.3) determine the electron densities of the $|e\gamma\rangle$ state,

$$\begin{aligned}
\rho_0(x,\vec{b}) &= \frac{\alpha m^2}{2\pi^2}\Big[\frac{1+x^2}{1-x}K_1^2(mb) + (1-x)K_0^2(mb)\Big] \\
\rho_x(x,\vec{b}) &= \rho_0(x,\vec{b}) + \frac{\alpha m^2}{\pi^2}\sin\phi_b\, x\, K_0(mb)K_1(mb)
\end{aligned} \tag{5.4}$$

The modified Bessel function behaves as $K_n(z) \simeq e^{-z}\sqrt{\pi/2z}$ for $z \to \infty$, and $K_0(z) \simeq \ln(1/z)$, $K_1(z) \simeq 1/z$ for $z \to 0$. The densities thus vanish rapidly as $b \gg 1/m$, and become more peaked at low $b \ll 1/m$ as $x \to 1$. However, the densities have broad distributions in b for all x (see Fig. 5.2). Because $\sum_i x_i\vec{b}_i = 0$, one might expect $\rho_0(x,\vec{b}) \to \delta^{(2)}(\vec{b})$ as $x \to 1$. The photon impact parameter $\vec{b}_\gamma = -x\vec{b}/(1-x) \to \infty$ as $x \to 1$, and therefore allows the density to remain wide. In QCD, color confinement would impose $\vec{b}_\gamma \lesssim 1/\Lambda_{\rm QCD}$, forcing $\vec{b} \to 0$ as $x \to 1$.

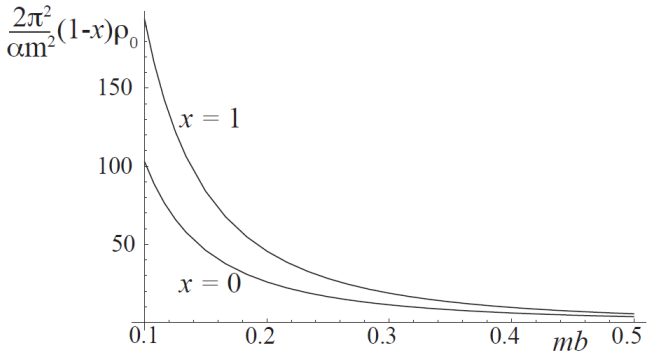

Figure 5.2: $\frac{2\pi^2}{\alpha m^2}(1-x)\rho_0(x,\vec{b})$ for $x=0$ and $x=1$. Note that the origin is at $b = 0.1/m$.

The spin of the electron is distributed among the constituents of the $|e\gamma\rangle$ Fock state. The Ji sum rule [12],

$$\frac{1}{2} = \frac{1}{2}\sum_q \Delta q + \sum_q L_q^z + J_g^z \tag{5.5}$$

expresses the $J^z = 1/2$ of the nucleon as a sum of the helicities $\frac{1}{2}\Delta q$ and orbital angular momenta L_q^z of quarks, and the angular momenta J_g^z of gluons, which are related to GPDs, and are thus in principle measurable. Alternative decompositions of the nucleon spin have been considered [50, 48], and there is controversy on how to split the angular momentum into separate quark and gluon contributions, and whether the gluon angular momentum can itself be split into spin and orbital parts [51]. We studied the expectation values of the electron helicity λ_e, the photon helicity λ_γ, and the orbital angular momentum $L_{e\gamma}^z = -i\partial_{\phi_b}$ of the $|e\gamma\rangle$ Fock state as functions of x and $\vec{b}$, defining the expectation value of the electron helicity λ_e for a parent electron with helicity λ as

$$\begin{aligned}\langle\lambda_e\rangle_\lambda &\equiv \frac{1}{N}\sum_{\lambda_e,\lambda_\gamma}\langle\lambda;\lambda_e,\lambda_\gamma|S_e^z|\lambda;\lambda_e,\lambda_\gamma\rangle \\ &= \frac{1}{2N}\sum_{\lambda_\gamma}\Big[|\psi^\lambda_{+,\lambda_\gamma}|^2 - |\psi^\lambda_{-,\lambda_\gamma}|^2\Big]\end{aligned} \tag{5.6}$$

which integrated over the impact parameter is proportional to the spin dependent $g_1(x)$ distribution. The expectation values of the photon helicity and orbital angular momentum are defined similarly. For $\lambda = +\frac{1}{2}$, we have

$$\begin{aligned}N\langle\lambda_e\rangle_+ &= \frac{\alpha m^2(1-x)}{8\pi^3}\frac{1}{2}\Big[(1+x^2)K_1^2(mb) - (1-x)^2K_0^2(mb)\Big] \\ N\langle\lambda_\gamma\rangle_+ &= \frac{\alpha m^2(1-x)}{8\pi^3}\Big[(1-x)^2K_1^2(mb) + (1-x)^2K_0^2(mb)\Big] \\ N\langle L_{e\gamma}^z\rangle_+ &= -\frac{\alpha m^2(1-x)}{8\pi^3}\Big[(1-x)^2K_1^2(mb)\Big]\end{aligned} \tag{5.7}$$

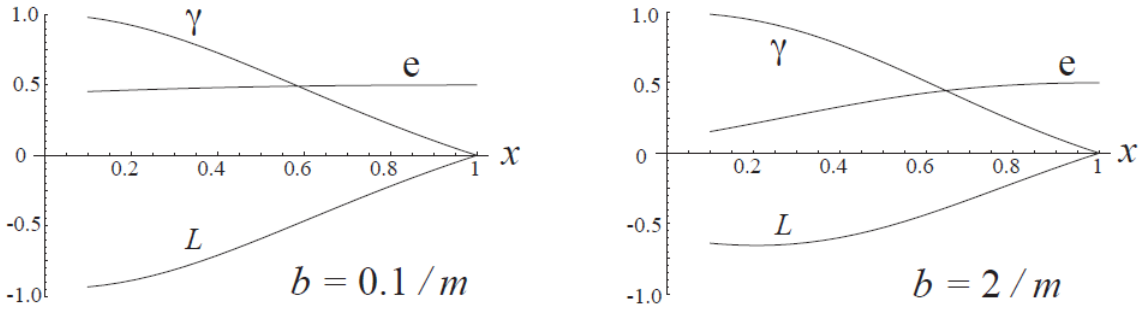

Figure 5.3: The expectation values $\langle\lambda_e\rangle_+$, $\langle\lambda_\gamma\rangle_+$ and $\langle L^z_{e\gamma}\rangle_+$ in the $|e\gamma\rangle$ Fock state as functions of the longitudinal momentum fraction x for $b = 0.1/m$ and $b = 2/m$.

where the normalization constant is

$$\begin{aligned} N &\equiv \sum_{\lambda_e,\lambda_\gamma} |\psi^+_{\lambda_e,\lambda_\gamma}|^2 \\ &= \frac{\alpha m^2(1-x)}{8\pi^3}\Big[(1+x^2)K_1^2(mb) + (1-x)^2K_0^2(mb)\Big] \end{aligned} \tag{5.8}$$

The expectation values (5.7) satisfy $\langle\lambda_e\rangle_+ + \langle\lambda_\gamma\rangle_+ + \langle L^z_{e\gamma}\rangle_+ = 1/2$, as expected. The x-dependence of each contribution is plotted in Fig. 5.3 for $b = 0.1/m$ and $b = 2/m$. As $x \to 1$, the electron carries all of the spin, while $\langle\lambda_\gamma\rangle_+$ and $\langle L^z_{e\gamma}\rangle_+$ vanish. For small x and b, the electron carries most of the spin, while $\langle\lambda_\gamma\rangle_+$ and $\langle L^z_{e\gamma}\rangle_+$ are large and cancel each other. We also studied the expectation value of the transverse spin for a transversely polarized electron,

$$\langle S^x_e\rangle_x \equiv \frac{1}{N}\sum_{\lambda_e,\lambda_\gamma}\langle S^x = \frac{1}{2};\lambda_e,\lambda_\gamma|S^x_e|S^x = \frac{1}{2};\lambda_e,\lambda_\gamma\rangle \tag{5.9}$$

which integrated over the impact parameter is proportional to the transverse spin distribution $h_1(x)$. Using $|S^x = +\frac{1}{2}\rangle = \Big[|\lambda = +\frac{1}{2}\rangle + |\lambda = -\frac{1}{2}\rangle\Big]/\sqrt{2}$ and $S^x_e|S^x = \frac{1}{2};\lambda_e,\lambda_\gamma\rangle = |S^x = \frac{1}{2};-\lambda_e,\lambda_\gamma\rangle$, we have

$$N\langle S^x_e\rangle_x = \frac{\alpha m^2(1-x)}{8\pi^3}\Big[x\,K_1^2(mb) + \sin\phi_b\,(1-x)K_0(mb)K_1(mb)\Big] \tag{5.10}$$

which is plotted in Fig. 5.4 for $b = 1/m$. The electron carries all of the transverse spin as $x \to 1$, while the contribution is $\propto x$ at small x. The results are qualitatively the same for all b.

5.2 Form factors from impact parameter densities

The transverse charge densities were expressed in terms of the form factors in (3.11) and (3.13). Using the closure of Bessel functions, the equations may be inverted,

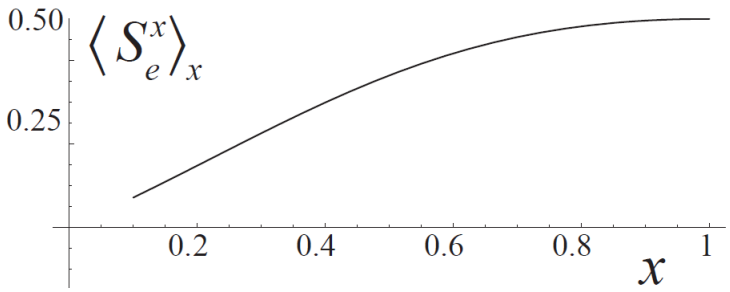

Figure 5.4: The expectation value $\langle S_e^x \rangle_x$ in the $|e\gamma\rangle$ Fock state as a function of the longitudinal momentum fraction x, integrated over ϕ_b and for $b = 1/m$.

$$\begin{aligned} F_1(Q^2) &= 2\pi \int_0^\infty db\, bJ_0(bQ)\rho_0(\vec{b}) \\ F_2(Q^2) &= \frac{2\pi m}{Q} \int_0^\infty db\, bJ_1(bQ)\Big(\rho_x^{\phi_b=\pi/2}(\vec{b}) - \rho_x^{\phi_b=3\pi/2}(\vec{b})\Big) \end{aligned} \tag{5.11}$$

which allowed us to study the transverse size of the Fock states contributing to the form factors at any Q^2. Similar studies have been made using GPD models for the nucleon [52, 53]. The general expectation is that only compact Fock states with $b \lesssim 1/Q$ contribute to the form factors as $Q^2 \to \infty$ at fixed x. Using (5.4), the order α form factors of the electron are

$$\begin{aligned} F_1(Q^2) &= \frac{\alpha m^2}{\pi} \int_0^1 dx \int_0^\infty db\, bJ_0(bQ)\Big[\frac{1+x^2}{1-x} K_1^2(mb) + (1-x)K_0^2(mb)\Big] \\ F_2(Q^2) &= \frac{4\alpha m^3}{\pi Q} \int_0^1 dx\, x \int_0^\infty db\, bJ_1(bQ)K_0(mb)K_1(mb) \end{aligned} \tag{5.12}$$

The Dirac form factor has the usual $1/(1-x)$ IR singularity and a logarithmic UV divergence, since $K_1(mb) \simeq 1/mb$ for $b \ll 1/m$. Renormalizing the UV divergence leaves a pointlike contribution to $F_1(Q^2)$, which is finite as $Q^2 \to \infty$. The low b approximation for the UV finite term, which is suppressed by m^2/Q^2 as $Q^2 \to \infty$, however diverges for large $b \equiv u/m$,

$$F_1(Q^2, b \to 0) \simeq \frac{\alpha}{\pi} \int_0^1 dx \int_0^\infty du\, J_0\Big(\frac{Q}{m}u\Big)\Big[\frac{1+x^2}{1-x}\frac{1}{u} + (1-x)u(\ln u)^2\Big] \tag{5.13}$$

signifying that only the leading contribution to $F_1(Q^2)$ at high Q^2 is restricted to small impact parameters. The low b approximation for the IR and UV finite Pauli form factor is ($t \equiv bQ$)

$$\begin{aligned} F_2(Q^2, b \to 0) &\simeq \frac{2\alpha m^2}{\pi Q^2} \int_0^\infty dt\, J_1(t) \ln\Big(\frac{Q}{m}\frac{1}{t}\Big) \\ &= \frac{\alpha m^2}{\pi Q^2} \ln\Big(\frac{Q^2}{m^2}\Big)\Big[1 + \mathcal{O}\Big(1/\ln(Q^2/m^2)\Big)\Big] \end{aligned} \tag{5.14}$$

which agrees with the leading $Q^2 \to \infty$ behavior of the standard result, signifying that only compact Fock states contribute to $F_2(Q^2)$ at high Q^2, even though the convergence to small

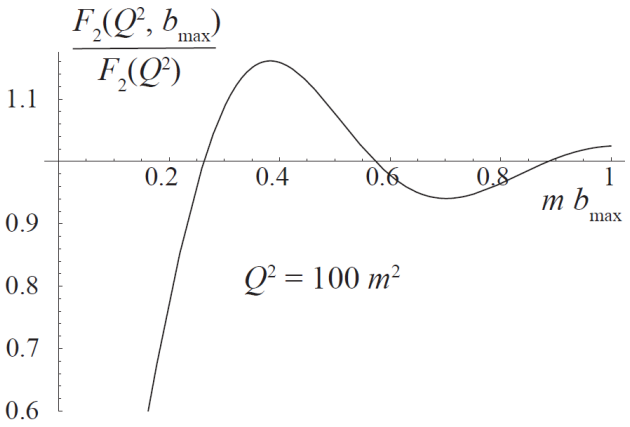

Figure 5.5: The ratio $F_2(Q^2, b_{\max})/F_2(Q^2)$, when the integral in (5.12) is restricted to $b \leq b_{\max}$ and $Q^2 = 100m^2$.

b is rather slow (see Fig. 5.5). The size distribution of the Fock states contributing to the form factors could affect the color transparency of quark fluctuations $q \to qg$ rescattering in a nucleus, where the rescattering amplitude is also weighted by size of the fluctuation $r_\perp = b/(1-x)$. When the b-integrals in (5.13) and (5.14) are multiplied by $b/(1-x)$, the b-integral in $F_2(Q^2)$ diverges, while the x-integral in $F_1(Q^2)$ diverges linearly at the endpoint $x = 1$. In contrast, in deeply exclusive meson production, $\gamma^*(Q^2)A \to MA$, the size of the Fock states is determined by the wave function of the virtual photon, which is proportional to $K_{0,1}(bQ)$, guaranteeing that the size distribution vanishes exponentially for $b \gtrsim 1/Q$ even after multiplied by any power of b. Color transparency is indeed seen in meson electroproduction [54], whereas the measurement of nucleon form factors in a nuclear environment failed to see evidence for color transparency [55].

According to (5.11), the anomalous magnetic moment is given by the charge density,

$$F_2(0) = \pi m \int_0^\infty db\, b^2 \Big(\rho_x^{\phi_b=\pi/2}(\vec{b}) - \rho_x^{\phi_b=3\pi/2}(\vec{b}) \Big) \tag{5.15}$$

which is an exact relation. This leads to an interesting, classical argument for the positivity of the electron anomalous magnetic moment, addressing a challenge already posed by Feynman [56]. Feynman called for more intuition on QED perturbative calculations, specifically noting that: "We have no physical picture by which we can easily see that the correction is roughly $\alpha/2\pi$, in fact, we do not even know why the sign is positive (other than by computing it)". Attemps have been made to answer this challenge by using dispersion theory in the non-relativistic limit [56], or by studying the effect of low-energy vacuum fluctuations on the electron [57]. Our qualitative argument is as follows. The charge density $\rho_x(\vec{b})$ measures the current $j^+ = j^0 + j^3$ of a particle at $x^+ = 0$ with spin in the x-direction. Then, for a classical spinning object, $j^3(y > 0) > 0$ while $j^3(y < 0) < 0$, and thus the density difference $\rho_x^{\phi_b=\pi/2}(\vec{b}) - \rho_x^{\phi_b=3\pi/2}(\vec{b}) > 0$ in (5.15) (see Fig. 5.6). A similar argument was used to understand the sign of the SSAs observed in semi-inclusive DIS [58].

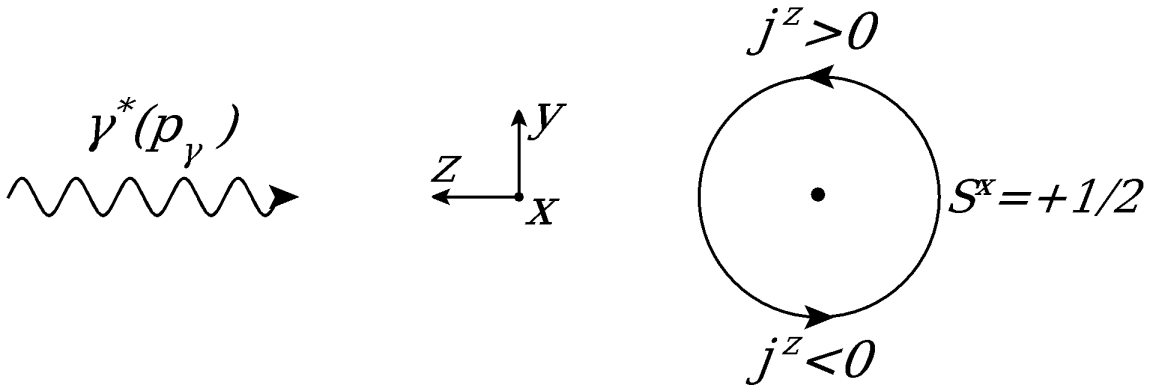

Figure 5.6: The current $j^z > 0$ and $j^z < 0$ for a classical spinning body with $L^x > 0$. The virtual photon measures $j^+ = j^0 + j^z$ at $x^+ = 0$, which is larger for $y > 0$ than for $y < 0$.

Chapter 6

Measuring transverse shape with virtual photons

Nucleon transverse charge densities are accessed via form factors measured in $\gamma^*(q)+N \to N$ with the resolution $b \sim 1/Q_{\max}$, as discussed in chapter 3. In paper III, we considered the prospects of measuring the transverse shape of any virtual photon induced process, $\gamma^*(q) + i \to f$, where the initial and final states can consist of several hadrons. Qualitative arguments concerning the size of such transitions have been used in the literature, but without quantitative verification. We showed how a specific Fourier transform of the $\gamma^*(q) + N \to f$ transition amplitude measures the transverse shape of the transition process, and is given by the overlap of the LF wave functions of the initial and final state. Only Fock states that are common to both the initial and final state contribute to the transition amplitude. The Fourier transformed cross section, on the other hand, reflects the difference between the impact parameters of the quark struck in the amplitude and its complex conjugate. We illustrated the method using examples with two-body final states.

6.1 Transverse shape of transition processes

The q-dependence of the virtual photon interaction in $\gamma^*(q) + N \to N$ provides information on the transverse densities of the nucleon, as discussed in chapter 3. In accordance with this and the electron microscopy analogy discussed in section 3.2, the q-dependence should provide information on the transverse shape and size of any virtual photon induced transition process, $\gamma^*(q) + i \to f$, where the initial and final states can consist of several particles. Such information could allow qualitatively new insight into strong interaction dynamics in transverse space. For example, in $\gamma^* N \to \pi N$, one expects the impact parameter distribution to narrow with the relative transverse momentum $k_\perp$ between the pion and the nucleon, since perturbative QCD predicts that the πN system has a small size at large momentum transfer. Such compactness of the πN system is suggested by the observed color transparency of high-energy pions dissociating into exclusive jets, where the measured A-dependence of the cross section agrees with the prediction for color transparency at high relative momentum $k_\perp$ [59, 60] (see Fig. 6.1). Large angle photoproduction cross sections are compatible with constituent counting rules, which predict that the energy dependence of the two-body exclusive reaction

k_t bin GeV/c	α	$\Delta\alpha$	α (CT)
1.25 – 1.5	1.64	+0.06 −0.12	1.25
1.5 – 2.0	1.52	±0.12	1.45
2.0 – 2.5	1.55	±0.16	1.60

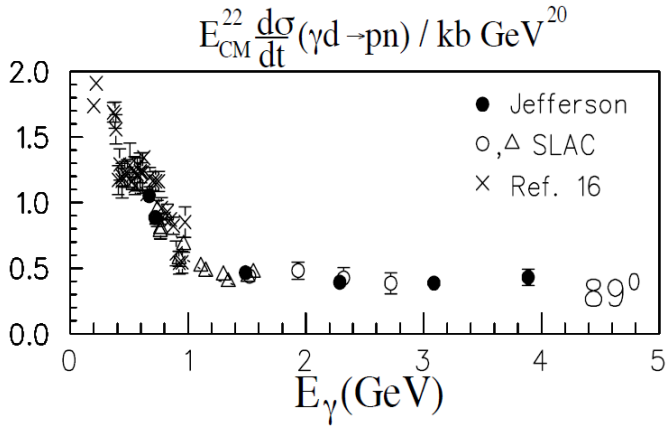

Figure 6.1: Left: The measured value and the color transparency prediction for the exponent α in the high-energy pion dissociation cross section $\sigma \propto A^\alpha$. Table from [60]. Right: The large angle photoproduction cross section $s^{11}d\sigma(\gamma D \to pn)/dt$ at $\theta_{cm} = 89°$ as function of the photon energy E_γ, showing the constituent counting rule behavior for $E_\gamma \gtrsim 1$ GeV. Figure from [66].

cross section is

$$\frac{d\sigma}{dt} = \frac{f(\theta_{cm})}{s^{n-2}} \tag{6.1}$$

where s and t are the usual Mandelstam variables, θ_{cm} is the center-of-mass angle and n denotes the number of elementary fields in the initial and final states [61, 62]. Thus, $n = 9$ for both $\sigma(\gamma p \to \pi^+ n)$ [63] and $\sigma(\gamma p \to K^+\Lambda)$ [64, 65], while $n = 13$ for $\sigma(\gamma D \to pn)$ [66] and $\sigma(\gamma\, ^3\mathrm{He} \to pp(n))$ [67] at $\theta_{cm} \simeq 90°$, which are satisfied by the data at surprisingly low energies (see Fig. 6.1). The constituent counting rules are based on perturbative QCD, signifying that the scattering Fock states are compact. Measuring the q^2-dependence of large angle electroproduction would allow to study the transverse size of the Fock states. High-energy diffractive processes such as $\gamma^* N \to \rho N$ (see [68] for a review) could allow the study of the impact parameter distributions of low x quarks, which are expected to be broader than for higher x quarks. In heavy quark production processes such as $\gamma^* N \to K\Lambda$ and $\gamma^* N \to D\Lambda_c$, the impact parameter distributions should narrow with the heavy quark mass, since both the creation and annihilation of heavy quarks has limited transverse range $\sim 1/m_q$.

6.2 Impact parameter analysis of $\gamma^* N \to f$

In the one-photon approximation, the lepton scattering amplitude is

$$M(lN \to l'f) = -e^2 \bar{u}(l')\gamma_\mu u(l)\frac{1}{q^2}\int d^4x\, e^{-iq\cdot x}\, \langle f(p_f)|J^\mu(x)|N(p)\rangle \tag{6.2}$$

To arrive at an interpretation in terms of the Fock states, we need to identify the $J^+(x)$ contribution in (6.2). For $l^- \to \infty$ with fixed q, the lepton part is $\bar{u}(l')\gamma_\mu u(l) = 2l^-\delta^-_\mu$, and the amplitude becomes

$$M(lN \to l'f) = -e^2\frac{l^-}{q^2}\langle f(p_f)|J^+(0)|N(p)\rangle(2\pi)^4\delta^{(4)}(p_f - p - q) \tag{6.3}$$

In analogy with the nucleon charge densities, the Fourier transform of the generalized form factor $\langle f(p_f)|J^+(0)|N(p)\rangle$ is done in a frame where

$$\begin{aligned} p &= (p^+, p^-, -\frac{1}{2}\vec{q}) \\ q &= (0^+, q^-, \vec{q}) \\ p_f &= (p^+, p^- + q^-, \frac{1}{2}\vec{q}) \end{aligned} \tag{6.4}$$

The transverse momentum eigenstates are expanded in impact parameter states using $|p^+, \vec{p}\rangle = 4\pi \int d^2\vec{b}\, e^{i\vec{p}\cdot\vec{b}}|p^+, \vec{b}\rangle$, and the excitation amplitude in impact parameter space is then

$$\begin{aligned} A_{fN}(\vec{b}) &\equiv \int \frac{d^2\vec{q}}{(2\pi)^2}\, e^{-i\vec{q}\cdot\vec{b}} \frac{1}{2p^+}\langle f(p_f)|J^+(0)|N(p)\rangle \\ &= \int \frac{d^2\vec{q}}{(2\pi)^2}\, d^2\vec{b}_N\, d^2\vec{b}_f\, e^{-i\vec{q}\cdot(\vec{b}+\vec{b}_N/2+\vec{b}_f/2)} \frac{(4\pi)^2}{2p^+}\langle f(p^+, \vec{b}_f)|J^+(0)|N(p^+, \vec{b}_N)\rangle \end{aligned} \tag{6.5}$$

The impact parameter states have the LF Fock expansions in terms of the impact parameter wave functions,

$$\begin{aligned} |p^+, \vec{b}\rangle_{x^+=0} &= \sum_n \prod_{i=1}^n \Big[\int_0^1 \frac{dx_i}{\sqrt{x_i}} \int 4\pi d^2\vec{b}_i\Big] \frac{1}{4\pi}\delta(1 - \sum_{i=1}^n x_i)\delta^{(2)}(\vec{b} - \sum_{i=1}^n x_i\vec{b}_i) \\ &\quad \times \psi_n(x_i, \vec{b}_i - \vec{b}) \prod_{i=1}^n b^\dagger(x_i p^+, \vec{b}_i) d^\dagger(...)a^\dagger(...)|0\rangle \end{aligned} \tag{6.6}$$

The electromagnetic current is $J^+(x) = e_q\bar{q}(x)\gamma^+ q(x) = 2e_q q_+^\dagger(x)q_+(x)$, where $q_+(x) = \frac{1}{4}\gamma^-\gamma^+ q(x)$, and the quark field is

$$q_+(0^+, x^-, \vec{x}) = \int \frac{dk^+}{k^+}\theta(k^+)\Big[b(k^+, \vec{x})u_+(k^+)e^{-ik^+x^-/2} + d^\dagger(k^+, \vec{x})v_+(k^+)e^{ik^+x^-/2}\Big] \tag{6.7}$$

where the operators at fixed transverse position $\vec{x}$ are $b(k^+, \vec{x}) = \int \frac{d^2\vec{k}}{16\pi^3} e^{i\vec{k}\cdot\vec{x}} b(k^+, \vec{k})$ and the spinors satisfy $u_+^\dagger(k^+, \lambda')u_+(k^+, \lambda) = k^+\delta_{\lambda',\lambda}$. The quark field eliminates an operator $b^\dagger(x_k p^+, \vec{b}_k)$ from (6.6) at $\vec{b}_k = \vec{x} = \vec{0}_\perp$ both in $|N\rangle$ and $|f\rangle$, and the remaining $n-1$ partons are thus identical in (6.5). The amplitude is diagonal in the number of Fock states, since a photon with $q^+ = 0$ cannot create a $q\bar{q}$ pair. The constraints $\sum_i x_i = 1$ force also the momentum fraction x_k of the struck quark to be the same, and the constraints $\vec{b} = \sum_i x_i\vec{b}_i$ require that the impact parameters of $|N\rangle$ and $|f\rangle$ are equal, $\vec{b}_f = \vec{b}_N$. The excitation amplitude in impact parameter space (6.5) becomes

$$\begin{aligned} A_{fN}(\vec{b}) &= \sum_n \prod_{i=1}^n \Big[\int_0^1 dx_i \int 4\pi d^2\vec{b}_i\Big] \frac{1}{4\pi}\delta(1 - \sum_{i=1}^n x_i)\delta^{(2)}(\sum_{i=1}^n x_i\vec{b}_i) \\ &\quad \times [\psi_n^f(x_i, \vec{b}_i)]^\dagger \psi_n^N(x_i, \vec{b}_i) \sum_k e_k\, \delta^{(2)}(\vec{b}_k - \vec{b}) \end{aligned} \tag{6.8}$$

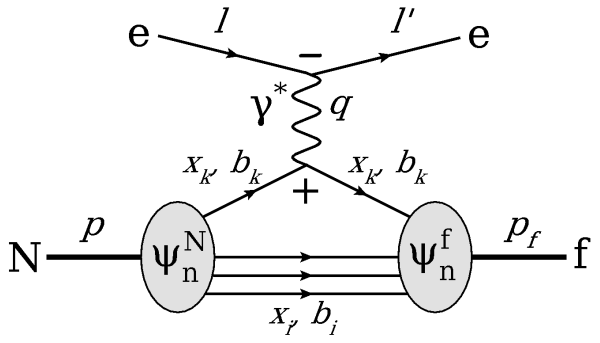

Figure 6.2: The J^+ electromagnetic current probes the Fock state of the $\gamma^* + N \to f$ transition. Only Fock states that are common to $|N\rangle$ and $|f\rangle$ contribute, and the amplitude in impact parameter space is given by the overlap of the LF wave functions ψ_n^N and ψ_n^f.

which thus gets contributions only from LF Fock states that are common to $|N\rangle$ and $|f\rangle$ which have a quark or antiquark at transverse position $\vec{b}_k = \vec{b}$ (see Fig. 6.2). The distribution in $\vec{b}$ provides information about the transverse size of the intermediate Fock states, which may be studied as a function of the final state $|f\rangle$. The amplitude $A_{fN}(\vec{b})$ is universal, in the sense that it depends only on the LF wave functions of $|N\rangle$ and $|f\rangle$, which are process independent. For $N = f$, the expression (6.8) reduces to the positive definite nucleon charge density $\rho_0(\vec{b})$ discussed in chapter 3.

6.3 Two-body final states

In the analysis of section 6.2, the final state can consist of several hadrons, $|f\rangle = |h_1, h_2 ... h_n\rangle$, and its momentum $p_f = p + q$ varies with the Fourier transform in (6.5). We are then free to specify the relative momenta of the hadrons, each one of which has its own Fock expansion. The multihadron Fock state may also be expanded using a LF Fock expansion in terms of the LF wave functions of the hadrons. For a pion-nucleon final state, in order to conform with the general Lorentz covariance of LF states,

$$|\pi N(p_f^+, \vec{p}_f; \psi^f)\rangle = \int_0^1 \frac{dx}{\sqrt{x(1-x)}} \int \frac{d^2\vec{k}}{16\pi^3} \psi^f(x, \vec{k}) |\pi(p_1) N(p_2)\rangle \tag{6.9}$$

where $\psi^f(x, \vec{k})$ is a freely chosen function of the relative variables x, $\vec{k}$ and

$$\begin{aligned} p_1^+ &= x p_f^+, & \vec{p}_1 &= x\vec{p}_f + \vec{k} \\ p_2^+ &= (1-x) p_f^+, & \vec{p}_2 &= (1-x)\vec{p}_f - \vec{k} \end{aligned} \tag{6.10}$$

Since x, $\vec{k}$ are independent of p_f, this defines the pion and nucleon momenta p_1, p_2 at all photon momenta q in the Fourier transform. If we fix the pion and nucleon momenta, the wave function ψ^f in (6.9) is a δ-function in x and $\vec{k}$. If we consider a resonance contribution to the amplitude, such as $\gamma^* N \to N^*(1440) \to \pi N$, the invariant mass of the πN state is

fixed,

$$p_f^2 = (p_1 + p_2)^2 = \frac{m_\pi^2}{x} + \frac{m_N^2}{1-x} + \frac{\vec{k}^2}{x(1-x)} = m_{N^*(1440)}^2 \tag{6.11}$$

and the excitation amplitude in impact parameter space (6.5) in the frame (6.4) is given by the $N \to N^*(1440)$ transition charge densities. If we do not specify an intermediate state, the $\gamma^* N \to \pi N$ amplitude can be expressed using six invariant amplitudes [69, 70], and the LF helicity amplitudes in impact parameter space (6.5) can be evaluated via a numerical Fourier transform using existing parametrisations of experimental data, and studied as functions of x and $\vec{k}$.

We studied the $l\mu \to l'\mu\gamma$ process as a QED example of a two-body final state. One of the helicity amplitudes for $\gamma^*\mu \to \mu\gamma$ expressed in terms of the relative variables is

$$A^{\mu\gamma,+(1/2)}_{+(1/2)+1}(\vec{q}; x, \vec{k}) = 2e\sqrt{x}\Big[\frac{\vec{e}_- \cdot \vec{k}}{(1-x)^2 m^2 + \vec{k}^2} - \frac{\vec{e}_- \cdot (\vec{k} - (1-x)\vec{q})}{(1-x)^2 + (\vec{k} - (1-x)\vec{q})^2}\Big] \tag{6.12}$$

where $\vec{e}_\lambda \cdot \vec{k} = -\lambda e^{i\lambda\phi_k}|\vec{k}|/\sqrt{2}$. The Fourier transform in (6.5) gives the amplitude for the virtual photon to interact with the muon at $\vec{b}$,

$$A^{\mu\gamma,+(1/2)}_{+(1/2)+1}(\vec{b}; x, \vec{k}) = 2e\sqrt{x}\Big[\frac{\vec{e}_- \cdot \vec{k}}{(1-x)^2 m^2 + \vec{k}^2}\delta^{(2)}(\vec{b}) - \frac{i}{2\sqrt{2}\pi}\frac{m\, e^{-i\phi_b}}{1-x}K_1(mb)\Big]\exp\Big(-i\frac{\vec{k}\cdot\vec{b}}{1-x}\Big) \tag{6.13}$$

The first term arises from the interaction with the initial state muon at $\vec{b} = 0$, and the second term reflects the impact parameter distribution of the final state muon in the $\mu\gamma$ state at $\vec{b} = 0$. Precisely the same result is obtained from the expression for the amplitude in terms of the $\mu \to \mu\gamma$ LF wave functions (6.8). Choosing the $\mu\gamma$ wave function $\psi^f(x, \vec{k})$ to correspond with a muon at fixed impact parameter $\vec{b}'_\mu$,

$$A^{\mu\gamma,+(1/2)}_{+(1/2)+1}(\vec{b}; x, \vec{b}'_\mu) = \sqrt{x(1-x)}\psi^+_{+(1/2)+1}(x, \vec{b}'_\mu)[-\delta^{(2)}(\vec{b}) + \delta^{(2)}(\vec{b} - \vec{b}'_\mu)] \tag{6.14}$$

Thus the virtual photon interacts with the initial muon at $\vec{b} = \vec{0}$ or the final muon at $\vec{b} = \vec{b}'_\mu$. We also considered the QED process $l\gamma^* \to l'\mu^-\mu^+$ with similar results.

6.4 Cross section in impact parameter space

The scattering amplitudes $\langle f(p_f)|J^+(0)|N(p)\rangle$ in the impact parameter space transition amplitude $A_{fN}(\vec{b})$ have nontrivial phases, and a partial wave analysis is possible only for a limited subset of all amplitudes, whereas the cross section is measurable. The Fourier transformed cross section for $lN \to l'f$ with $l^- \to \infty$ at fixed momentum transfer $q = l - l'$ is proportional to

$$\begin{aligned} S_{fN}(\vec{b}) &= \int \frac{d^2\vec{q}}{(2\pi)^2} e^{-i\vec{q}\cdot\vec{b}} |\frac{1}{2p^+}\langle f(p_f)|J^+(0)|N(p)\rangle|^2 \\ &= \int d^2\vec{b}_q\, A_{fN}(\vec{b}_q) A^*_{fN}(\vec{b}_q - \vec{b}) \end{aligned} \tag{6.15}$$

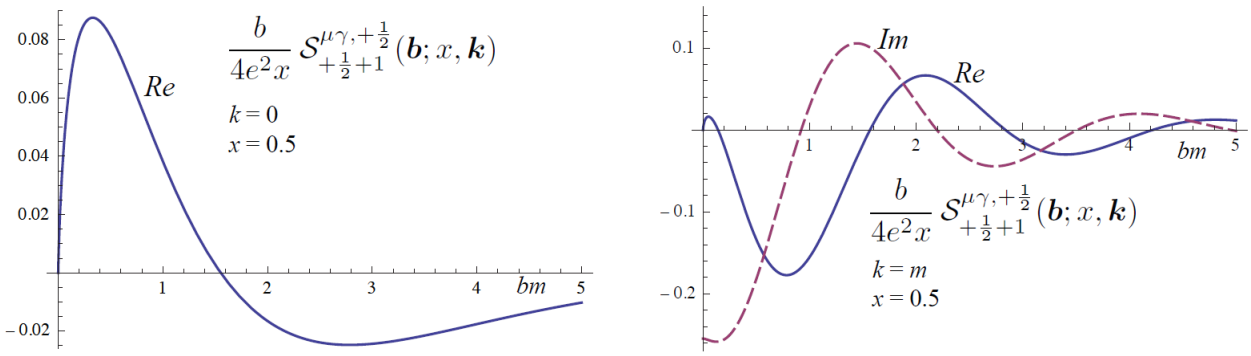

Figure 6.3: The real and imaginary parts of the Fourier transformed cross section $bS^{\mu\gamma,+(1/2)}_{+(1/2)+1}(\vec{b};x,\vec{k})$ for $\gamma^*\mu\to\mu\gamma$ with $\vec{k}||\vec{b}$.

Thus the $\vec{b}$-distribution in the Fourier transformed cross section reflects the difference between the impact parameters of the quark struck in the amplitude and its complex conjugate. The cross section has a real part that is even under $\vec{b}\to-\vec{b}$, and an imaginary part that is odd, which vanishes if the squared matrix element in (6.15) is invariant under $\vec{q}\to-\vec{q}$. A nonvanishing imaginary part can be caused by a correlation with $\vec{q}$ and a transverse direction defined by the final state f, such as a transverse momentum or polarization. For $|f\rangle=|\pi(p_1)N(p_2)\rangle$ discussed in section 6.3, the cross section is a function of the relative variables x and $\vec{k}$,

$$\int\frac{d^2\vec{q}}{(2\pi)^2}e^{-i\vec{q}\cdot\vec{b}}\vec{q}^4\frac{d\sigma(lN\to l'\pi N)}{d^2\vec{q}\,dx\,d^2\vec{k}}=\frac{\alpha^2}{4\pi^3}\frac{1}{x(1-x)}S_{\pi N,N}(\vec{b};x,\vec{k}) \tag{6.16}$$

For the QED example $\gamma^*\mu\to\mu\gamma$, where the impact parameter space amplitude is given by (6.13),

$$\begin{aligned}S^{\mu\gamma,+(1/2)}_{+(1/2)+1}(\vec{b};x,\vec{k}) &= 4e^2x\Big[\frac{\vec{k}^2/2}{(1-x)^2m^2+\vec{k}^2}\delta^{(2)}(\vec{b})-im\frac{|\vec{k}|\cos(\phi_b-\phi_k)}{(1-x)^2m^2+\vec{k}^2}\frac{K_1(mb)}{2\pi(1-x)}\\ &\quad+\frac{K_0(mb)-\frac{1}{2}mbK_1(mb)}{4\pi(1-x)^2}\Big]\exp\Big(-i\frac{\vec{k}\cdot\vec{b}}{1-x}\Big)\end{aligned} \tag{6.17}$$

which is plotted in Fig. 6.3. The three terms in (6.17) correspond to 2, 1, and 0 of the virtual photon interactions occurring on the initial muon, and the imaginary part arises from the correlation between $\vec{b}$ and $\vec{k}$.

Chapter 7

Conclusions and outlook

High-energy scattering experiments provide a window for studying hadron structure and QCD dynamics. The parton picture of the hadron is obtained by using the method of LF quantization. The division of momentum, spin and charge between the partons in the hadron are described by measurable distribution functions. In this thesis, I discussed both inclusive and exclusive scattering processes, in which these distributions are accessible.

Parton distributions are generally accessed via QCD factorization, which is based on the incoherence between the soft and hard dynamics in the scattering process. Factorization is valid in the Bjorken limit of hard processes, in which $Q^2 \to \infty$ and the LF energy q^- of the photon increases as $q^- \propto Q^2$. Only one parton in each hadron takes part in the hard subprocess in the Bjorken limit. Coherence effects are, however, expected and observed when one of the active partons carries $x \to 1$. In paper I, we defined and studied the BB limit of $Q^2 \to \infty$ with $Q^2(1-x)$ fixed, concentrating on the DY process $\pi N \to \mu^-\mu^+ + X$, where x is the momentum fraction of the pion carried by the lepton pair. We showed that a new kind of factorization holds in the BB limit. The virtual photon polarization is longitudinal rather than transverse in the DY process, and the cross section is proportional to a multiparton distribution, which would be of higher twist in the standard Bjorken limit. The DY amplitudes follow simple helicity systematics in the BB limit.

Generalized parton distributions (GPDs) contain information on the transverse distribution of quarks, but their measurement is more involved than those of the standard parton distributions measured in inclusive processes. The transverse charge densities are defined as Fourier transforms of the electromagnetic form factors, a connection that has attracted considerable interest in recent years. The form factors are well defined at all Q^2, and are much easier to measure than the GPDs, which has allowed to plot the nucleon charge densities model independently. In paper II, we applied these methods to the QED electron by studying the form factors, charge densities and spin distributions of the $|e\gamma\rangle$ Fock state in impact parameter space. Only transversally compact Fock states contribute to the leading behavior of the Dirac and Pauli form factors. The Fock state conserves the spin of the electron, while the separate contributions from the helicities and orbital angular momentum of the constituents depend on the impact parameter and longitudinal momentum fraction. We showed that the sign of the electron anomalous magnetic moment can be understood intuitively from the transverse densities.

Nucleon transverse charge densities are accessed via form factors measured in $\gamma^*(q)+N \to$

N. In paper III, we considered the transverse shape of any virtual photon induced transition process, $\gamma^*(q) + i \to f$, where the initial and final states can consist of several hadrons. Qualitative arguments concerning the size of such processes have been used in the literature, but without quantitative verification. We showed how a specific Fourier transform of the $\gamma^*(q) + N \to f$ transition amplitude measures the transverse shape of the transition process, and is given by the LF wave functions of the nucleon and the final state. The Fourier transformed cross section reflects the difference between the impact parameters of the quark struck in the amplitude and its complex conjugate.

The relevance of the BB limit to other high x processes merits further study. It has been shown that a large transverse single-spin asymmetry of $\mathcal{O}(1)$ in $pp^\uparrow \to \pi(x_F, k_\perp) + X$ can arise in the BB limit, but factorization analogous to the one considered in paper I is needed for a quantitative analysis. The generalized charge densities considered in paper III have several avenues of application, as discussed in chapter 6. As a first study, the existing parametrisations of experimental data on $\gamma^* N \to \pi N$ would allow a study of the transverse extent of the transition process as a function of the relative momentum between the nucleon and the pion.

Bibliography

[1] F. Butler, H. Chen, J. Sexton, A. Vaccarino, and D. Weingarten. *Nucl. Phys.*, B430:179–228, 1994. arXiv:hep-lat/9405003.

[2] S. Aoki et al. *Phys. Rev. Lett.*, 84:238–241, 2000. arXiv:hep-lat/9904012.

[3] M. Gell-Mann. *Phys. Lett.*, 8:214–215, 1964.

[4] G. Zweig. (CERN-TH-412):80 p, Feb 1964.

[5] G. Sterman et al. *Rev. Mod. Phys.*, 67(1):157–248, Jan 1995.

[6] J.C. Collins, D.E. Soper, and G.F. Sterman. *Adv. Ser. Direct. High Energy Phys.*, 5:1–91, 1988. arXiv:hep-ph/0409313.

[7] K. Nakamura et al. *J. Phys.*, G37:075021, 2010.

[8] S.J. Brodsky, P. Hoyer, N. Marchal, S. Peigne, and F. Sannino. *Phys. Rev.*, D65:114025, 2002. arXiv:hep-ph/0104291.

[9] V. Barone, F. Bradamante, and A. Martin. *Prog. Part. Nucl. Phys.*, 65:267–333, 2010. arXiv:1011.0909 [hep-ph].

[10] J. Collins and J-W. Qiu. *Phys. Rev.*, D75:114014, 2007. arXiv:0705.2141 [hep-ph].

[11] M. Diehl. *Phys. Rept.*, 388:41–277, 2003. arXiv:hep-ph/0307382.

[12] X-D. Ji. *Phys. Rev. Lett.*, 78:610–613, 1997. arXiv:hep-ph/9603249.

[13] A.V. Belitsky, D. Mueller, and A. Kirchner. *Nucl. Phys.*, B629:323–392, 2002. arXiv:hep-ph/0112108.

[14] S.J. Brodsky, H-C. Pauli, and S.S. Pinsky. *Phys. Rept.*, 301:299–486, 1998. arXiv:hep-ph/9705477.

[15] R.W. Mcallister and R. Hofstadter. *Phys. Rev.*, 102:851–856, 1956.

[16] W.M. Alberico, S.M. Bilenky, C. Giunti, and K.M. Graczyk. *Phys. Rev.*, C79:065204, 2009. arXiv:0812.3539 [hep-ph].

[17] S.D. Drell and T-M. Yan. *Phys. Rev. Lett.*, 24(4):181–186, Jan 1970.

[18] M.G. Rocha, F.J. Llanes-Estrada, D. Schuette, and S.V. Chavez. *Eur. J. Phys.*, A44:411, 2010. arXiv:0910.1448 [hep-ph].

[19] M. Burkardt. *Phys. Rev.*, D62:071503, 2000. arXiv:hep-ph/0005108.

[20] M. Burkardt. *Int. J. Mod. Phys.*, A18:173–208, 2003. arXiv:hep-ph/0207047.

[21] D. Chakrabarti, R. Manohar, and A. Mukherjee. *Phys. Lett.*, B682:428–434, 2010. arXiv:0908.4315 [hep-ph].

[22] D.E. Soper. *Phys. Rev.*, D15:1141, 1977.

[23] G.A. Miller. *Phys. Rev. Lett.*, 99(11):112001, Sep 2007.

[24] J. Arrington, W. Melnitchouk, and J.A. Tjon. *Phys. Rev.*, C76:035205, 2007.

[25] R. Bradford, A. Bodek, H.S. Budd, and J. Arrington. *Nucl. Phys. Proc. Suppl.*, 159:127–132, 2006. arXiv:hep-ex/0602017.

[26] J.J. Kelly. 2001. arXiv:hep-ph/0111251.

[27] C.E. Carlson and M. Vanderhaeghen. *Phys. Rev. Lett.*, 100:032004, 2008. arXiv:0710.0835 [hep-ph].

[28] L. Tiator and M. Vanderhaeghen. *Phys. Lett.*, B672:344–348, 2009. arXiv:0811.2285 [hep-ph].

[29] J. Blumlein and H. Bottcher. *Phys. Lett.*, B662:336–340, 2008. arXiv:0802.0408 [hep-ph].

[30] K.J. Anderson et al. *Phys. Rev. Lett.*, 43(17):1219–1222, Oct 1979.

[31] J.P. Alexander et al. *Phys. Rev. D*, 34(1):315–317, Jul 1986.

[32] E.L. Berger and S.J. Brodsky. *Phys. Rev. Lett.*, 42(15):940–944, Apr 1979.

[33] C. Biino et al. *Phys. Rev. Lett.*, 58(24):2523–2526, Jun 1987.

[34] D.L. Adams et al. *Phys. Lett.*, B264:462–466, 1991.

[35] A. Bravar et al. *Phys. Rev. Lett.*, 77(13):2626–2629, Sep 1996.

[36] P. Hoyer and M. Järvinen. *JHEP*, 02:039, 2007. arXiv:hep-ph/0611293.

[37] W. Melnitchouk, R. Ent, and C. Keppel. *Phys. Rept.*, 406:127–301, 2005. arXiv:hep-ph/0501217.

[38] J.D. Bjorken and J. Kogut. *Phys. Rev. D*, 8(5):1341–1357, Sep 1973.

[39] P. Hoyer. 2003. arXiv:hep-ph/0307263.

[40] E.R. Berger, M. Diehl, and B. Pire. *Phys. Lett.*, B523:265–272, 2001. arXiv:hep-ph/0110080.

[41] J.C Collins, L. Frankfurt, and M. Strikman. *Phys. Rev.*, D56:2982–3006, 1997. arXiv:hep-ph/9611433.

[42] R.L. Jaffe. *Nucl. Phys.*, B229:205, 1983.

[43] B. Pire and L. Szymanowski. *Phys. Lett.*, B622:83–92, 2005. arXiv:hep-ph/0504255.

[44] S.J. Brodsky, D.S. Hwang, B-Q. Ma, and I. Schmidt. *Nucl. Phys.*, B593:311–335, 2001. arXiv:hep-th/0003082.

[45] S.J. Brodsky, M. Diehl, and D.S. Hwang. *Nucl. Phys.*, B596:99–124, 2001. arXiv:hep-ph/0009254.

[46] D. Chakrabarti and A. Mukherjee. *Phys. Rev. D*, 71(1):014038, Jan 2005.

[47] S.J. Brodsky, D. Chakrabarti, A. Harindranath, A. Mukherjee, and J.P. Vary. *Phys. Rev. D*, 75(1):014003, Jan 2007.

[48] M. Burkardt and H. BC. *Phys. Rev.*, D79:071501, 2009. arXiv:0812.1605 [hep-ph].

[49] S.J. Brodsky and S.D. Drell. *Phys. Rev. D*, 22(9):2236–2243, Nov 1980.

[50] R.L. Jaffe and A. Manohar. *Nucl. Phys.*, B337:509–546, 1990.

[51] E. Leader. *Phys. Rev.*, D83:096012, 2011. arXiv:1101.5956 [hep-ph].

[52] M. Diehl, T. Feldmann, R. Jakob, and P. Kroll. *Eur. Phys. J.*, C39:1–39, 2005. arXiv:hep-ph/0408173.

[53] M. Guidal, M.V. Polyakov, A.V. Radyushkin, and M. Vanderhaeghen. *Phys. Rev. D*, 72(5):054013, Sep 2005.

[54] A. Airapetian et al. *Phys. Rev. C*, 66(4):044613, Oct 2002.

[55] K. Garrow et al. *Phys. Rev. C*, 66(4):044613, Oct 2002.

[56] S.D. Drell and H.R. Pagels. *Phys. Rev.*, 140(2B):B397–B407, Oct 1965.

[57] J. Dupont-Roc, C. Fabre, and C. Cohen-Tannoudji. *Journal of Physics B: Atomic and Molecular Physics*, 11(4):563, 1978.

[58] M. Burkardt. *Phys. Rev. D*, 66(11):114005, Dec 2002.

[59] E.M. Aitala et al. *Phys. Rev. Lett.*, 86(21):4768–4772, May 2001.

[60] E.M. Aitala et al. *Phys. Rev. Lett.*, 86(21):4773–4777, May 2001.

[61] S.J. Brodsky and G.R. Farrar. *Phys. Rev. Lett.*, 31(18):1153–1156, Oct 1973.

[62] V.A. Matveev, R.M. Muradian, and A.N. Tavkhelidze. *Nuovo Cim. Lett.*, 7:719–723, 1973.

[63] R.L. Anderson et al. *Phys. Rev. D*, 14(3):679–697, Aug 1976.

[64] M.E. McCracken et al. *Phys. Rev. C*, 81(2):025201, Feb 2010.

[65] R.A. Schumacher and M.M. Sargsian. *Phys. Rev. C*, 83(2):025207, Feb 2011.

[66] C. Bochna et al. *Phys. Rev. Lett.*, 81(21):4576–4579, Nov 1998.

[67] I. Pomerantz et al. *Phys. Lett.*, B684:106–109, 2010. arXiv:0908.2968 [nucl-ex].

[68] M. Wusthoff and A.D. Martin. *J. Phys.*, G25:R309–R344, 1999. arXiv:hep-ph/9909362.

[69] F.A. Berends, A. Donnachie, and D.L. Weaver. *Nucl. Phys.*, B4:1–53, 1967.

[70] B. Pasquini, D. Drechsel, and L. Tiator. *Eur. Phys. J.*, A34:387–403, 2007. arXiv:0712.2327 [hep-ph].